EFFECT OF VOIDS ON THE CRACK KINKING IN SINGLE LAP JOINTS

A Thesis

by

AHMED MOSTAFA ABOELMAHASEN ELSAYED SENGAB

Submitted to the Office of Graduate and Professional Studies of
Texas A&M University
in partial fulfillment of the requirements for the degree of

MASTER OF SCIENCE

Chair of Committee,	Ramesh Talreja
Committee Members,	Terry Creasy
	Mohammad Naraghi
Head of Department,	Ibrahim Karaman

May 2015

Major Subject: Material Science and Engineering

ABSTRACT

Polymer matrix composites are used extensively for their exceptional mechanical properties. The effect of voids on the energy release rate of interface crack has been studied before; however none of the studies investigated the effect of voids on the kinking of a crack from the interface into the adhesive film.

In the following report, a parametric study is conducted to understand the effect of the void size, the void shape and the void location on the kinking of an interface crack in single lap joint. An interface crack can originate from the maximum shear stress or the maximum normal stress that occurs at the interface between the adherend and the adhesive. A void is placed ahead of the crack tip at various distances in the Finite elements model to determine the critical distance. After determining the critical distance, the effect of the void radius and the void shape are examined on the crack kinking process. The interface crack is assumed to propagate a distance of 0.1mm at different angles ranging from 0 to 90 degrees with an increment of 10 degrees. The energy release rate is calculated by the revised virtual crack closure technique (RVCCT). The total energy release rate is calculated by adding Mode I and Mode II from the revised virtual crack closure technique (RVCCT) and justified by the J-integral method. Since the crack is an interface crack, the crack is expected to have a mixed mode behavior. A force boundary condition is applied. As the force increases, Mode I and Mode II increase. Moreover, it is evident from the results obtained that a void could lead an interface crack to kink into the adhesive, if the distance between the void and crack tip is significantly small to cause an interaction between the crack tip and the void.

DEDICATION

To Dina and Mostafa

ACKNOWLEDGMENTS

A few years ago, I would have never thought that I would be here at Texas A&M University. For that, I would like to thank ALLAH for his support and guiding me through the adversities of life.

On a different note, I would like to thank Professor Talreja for helping me in attending Texas A&M University. Also, without Professor Talreja support and guidance this work would not have been possible. Moreover, I would like to think Professor Talreja for his efforts and advice, his support was always a driving force during my studies.

Apart from my advisor, there are many people who contributed to my advancement through my studies at Texas A&M. First and utmost I would like to thank my father, my mother, my brother and my sister for always pushing me forward and helping me trying to achieve my best.

In addition, I would like to thank my father in law, my mother in law, my brother in law and my sister in law for treating me as a part of their family. I have always felt that I am a member of their family.

Also, I must thank Khaled Maala for his help during my course of study, for his support and for the good times that we have spent together.

Finally, I would like to thank my wife -Dina- for supporting me during my good and bad times. I would not have reached this far without her tolerance and support

NOMENCLATURE

	Shear stress
P	Force per unit width
c	Half of the adhesive bond length
E_u	Elastic modulus of upper adhered for unsymmetrical adherends
t_u	Thickness of upper adherend for unsymmetrical adherends
E_l	Elastic modulus of lower adhered for unsymmetrical adherends
t_l	Thickness of lower adhered for unsymmetrical adherends
E	Elastic modulus of upper and lower adhered for symmetrical adherends
t	Thickness of upper and and lower adhered for symmetrical adherends
E_a	Elastic modulus of the adhesive
G_a	Shear modulus of the adhesive
t_a	Thickness of the adhesive bonds
l	Adherend length without the adhesive bond overlap
ν	Poisson ratio of the adherend
σ	Peel or normal stress
M_1	Moment in the upper adherend
M_2	Moment in the adhesive layer
V_1	Shear force in the upper adherend
k	Load eccentricity factor
D_1	Rigidity of the upper adherend
D_2	Rigidity of the adhesive bond including upper and lower adherends
G_I	Mode I energy release rate
G_{II}	Mode II energy release rate

G_{IIV}	Mode II energy release rate with void
G_T	Total energy release rate
d1	Horizontal distance of void from the crack tip
2c	Adhesive bond length
R	Void radius
F	Void length (elongated void case)
VCCT	Virtual crack closure technique
RVCCT	Revised virtual crack closure technique

TABLE OF CONTENTS

Page

LIST OF FIGURES

FIGURE Page

LIST OF TABLES

CHAPTER I

INTRODUCTION

Adhesive bonded joints are widely used in both aerospace and automotive industries. These joints are usually preferred as a joining mechanism over other mechanisms such as: Bolting, riveting and welding. For example, riveting or bolting is not a favorable joining mechanism for fiber-reinforced composites, as the exceptional mechanical properties of these composites will be deteriorated as a result of the induced damage due to bolting or riveting. Moreover, welding is not an applicable joining mechanism of fiber-reinforced composites. There are various types of adhesive bonded joints, For example, single lap joints, double lap joints and tapered lap joints [1]. Fig. 1, Fig. 2 and Fig. 3 illustrate the geometry of the single lap joint, double lap joint and tapered lap joint respectively. The choice between different types of joints depends on the application as well as the manufacturing costs. For instance, single lap joints are the easiest to manufacture and therefore has the lowest cost, however under the same loading conditions the single lap joint has the highest stress when compared to other types of joints. Adams and Peppiatt [2] showed that the failure load of a single lap joint is approximately half the failure load of a double lap joint. Also, Adams and Peppiatt [2] showed that the maximum principal stress in a double lap joint is approximately half the maximum principal stress in a single lap joint.

Fig. 1 Single lap joint geometry [1].

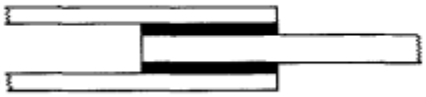

Fig. 2 Double lap joint geometry [1].

Fig. 3 Tapered lap joint geometry [1].

Single lap joints have the lowest failure load due to the load eccentricity reported by Goland and Ressiner [3], which increase the normal and the shear stress in the adhesive layer of the single lap joint compared to the double lap joint. Although, there are various types of joints, the main focus of this report will be only on single lap joints.

I.A- Motivation

I.A.1- Mechanics of single lap joints

The Volkersen model was the first analytical model to determine the shear stress within the adhesive layer of a single lap joint. The Volkersen model was developed in 1939 and it is based on the following assumptions [4]:

- The load is transferred from the adherends to the adhesive by a shear lag mechanism
- The adhesive is in shear and the adherends are in tension
- The shear stress is constant across the thickness of the adhesive layer
- The maximum shear deformation and the maximum shear stress is at the ends of the adhesive layer as shown in Fig. 4 i.e: points C and D

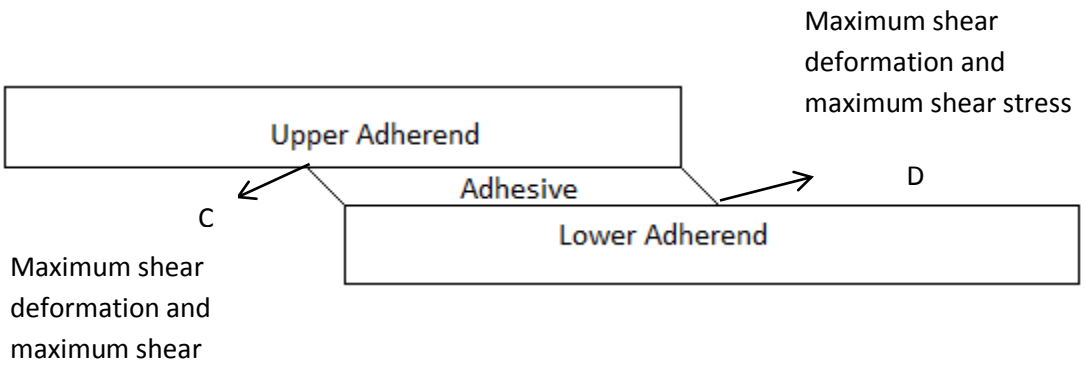

Fig. 4 Deformation of a single lap joint based on the volkersen model.

Equation (1) shows the shear stress distribution within the adhesive layer based on the Volkersen model.

$$\tau = \frac{\lambda P}{4}\left(\frac{\cosh(\lambda x)}{\sinh(\lambda c)} - \frac{E_u t_u - 2E_l t_l}{E_u t_u + 2E_l t_l}\frac{\sinh(\lambda x)}{\cosh(\lambda c)}\right) \tag{1}$$

$$\lambda^2 = \frac{G_a}{t_a}\left(\frac{1}{E_l t_l} + \frac{2}{E_u t_u}\right) \tag{2}$$

For symmetric single lap joints, where the upper and lower adherends are of the same material and of the same geometry, equations (1) and (2) reduce to the following:

$$\tau = \frac{\lambda p}{4}\left(\frac{\cosh(\lambda x)}{\sinh(\lambda c)} + \frac{1}{3}\frac{\sinh(\lambda x)}{\cosh(\lambda c)}\right) \tag{3}$$

$$\lambda^2 = \frac{G_a}{t_a}\left(\frac{3}{Et}\right) \tag{4}$$

Contrary to the Volkersen model, the eccentric load path shown in Fig. 5 was taken into consideration by Goland and Reissner [3], which lead to the normal (peel) stress. Goland and Reissner [3] developed their model for both inextensible and extensible adhesives, however for the sake of interest only extensible adhesive will be taken into consideration. Goland and Reissner [3] derived the shear stress and the normal stress equations based on the classical beam theory. The upper adherend, the lower adherend and the adhesive layer are treated as separate beams with appropriate boundary conditions applied.

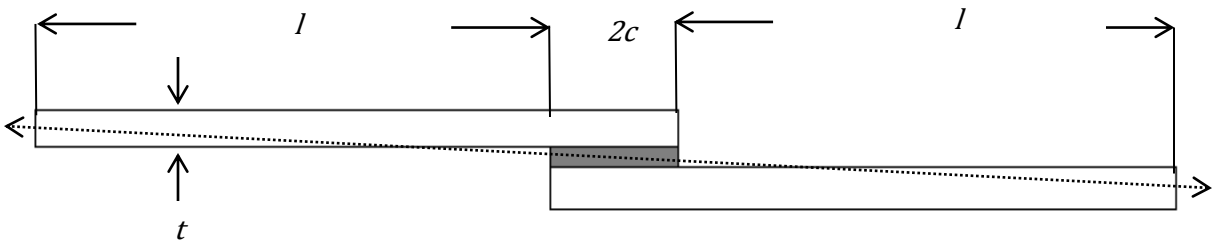

Fig. 5 Geometry of the single lap joint.

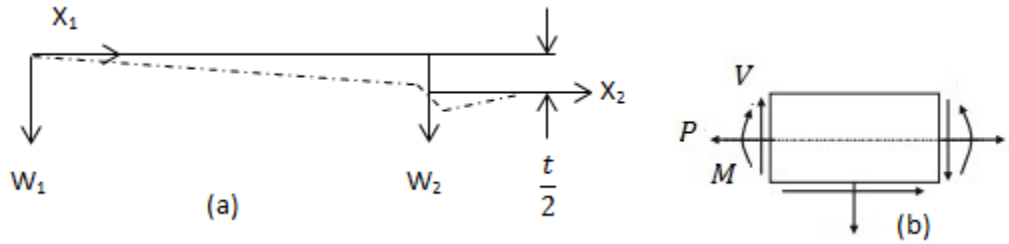

Fig. 6 a) Neutral axis of the upper adherend (X_1-W_1) and the adhesive (X_2-W_2) before deformation (solid line) and after deformation (dashed line) b) positive convention for moment, shear force and axial force [3].

Goland and Ressiner [3] showed that the moment in the upper adherend as shown in Fig. 6 is equal to the following:

$$M_1 = P(\alpha_n x_1 - w_1) \quad 0 \le x_1 \le l \tag{5}$$

$$\alpha_n = \frac{1}{2}\left(\frac{t}{l+c}\right) \tag{6}$$

Also, Goland and Reissner [3] showed that the moment in the adhesive layer is equal to the following:

$$M_2 = P\left(\alpha_n(x_2 + l) - w_2 - \frac{t}{2}\right) \quad 0 \le x_2 \le c \tag{7}$$

From simple beam theory Goland and Reissner [3] showed the following:

$$\frac{d^2w_1}{dx_1{}^2} = -\frac{M_1}{D_1} = \frac{P(\alpha_n x_1 - w_1)}{D_1} \tag{8}$$

$$\frac{d^2w_2}{dx_2{}^2} = -\frac{M_2}{D_2} = \frac{P\left(\alpha_n(x_2 + l) - w_2 - \frac{t}{2}\right)}{D_2} \tag{9}$$

$$D_1 = \frac{D_2}{8} = \frac{Et^3}{12(1-\nu^2)} \tag{10}$$

Equations (8) and (9) are second order differential equations that have a general solution and the constants are calculated using the following boundary conditions:

$$x_1 = 0 \qquad w_1 = 0 \tag{11.a}$$

$$x_1 = l\,, x_2 = 0 \qquad w_1 = w_2 \tag{11.b}$$

$$x_1 = l\,, x_2 = 0 \qquad \frac{dw_1}{dx_1} = \frac{dw_2}{dx_2} \tag{11.c}$$

$$x_2 = c \qquad w_2 = 0 \tag{11.d}$$

By solving equations (8) and (9) and applying the boundary conditions in (11) Goland and Reissner [3] showed that the moment and the shear force at the transition i.e: $x_1 = l$ is the following:

$$M_o = M_1(x_1 = l) = \frac{Pt}{2}\left(\frac{(\cosh(u_2 c))(\sinh(u_1 l))}{(\cosh(u_2 c))(\sinh(u_1 l)) + \frac{u_1}{u_2}(\cosh(u_1 l))(\sinh(u_2 c))}\right) \tag{12}$$

$$V_o = V_1(x_1 = l) = \frac{Pt}{2}\left(\frac{(\cosh(u_2 c))(\cosh(u_1 l))}{(\cosh(u_2 c))(\sinh(u_1 l)) + \frac{u_1}{u_2}(\cosh(u_1 l))(\sinh(u_2 c))}\right) \quad (13)$$

$$u_1 = \sqrt{\frac{P}{D_1}} \quad \& \quad u_2 = \sqrt{\frac{P}{D_2}} \quad (14)$$

The adherend and the adhesive are treated as separate beams. Goland and Reissner [3] derived an expression for the shear stress and the normal stress, Fig.7, by applying the appropriate boundary conditions. The distribution of the stresses across the adhesive layer is the following:

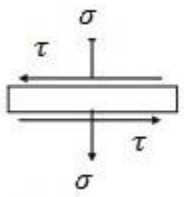

Fig. 7 Shear and normal stress in adhesive layer [3].

$$\tau = \frac{-P}{8c}\left(\frac{\beta c}{t}(1+3k)\left(\frac{(\cosh(\frac{\beta x}{t}))}{(\sinh(\frac{\beta c}{t}))}\right) + 3(1-k)\right) \quad (15)$$

$$\sigma = \frac{Pt}{\Delta c^2}((R_2\gamma^2 + \gamma k' \cosh\gamma\cos\gamma)\cosh\gamma\frac{x}{c}\cos\gamma\frac{x}{c} + \left(R_1\gamma^2\frac{k}{2} + \gamma k'\sinh\gamma\sin\gamma\right)\sinh\gamma\frac{x}{c}\sin\gamma\frac{x}{c}) \quad (16)$$

$$\beta^2 = 8\frac{G_a t}{E t_a} \quad (17)$$

$$k = 2\frac{M_o}{Pt} \quad (18)$$

$$\gamma = \sqrt[4]{\frac{6E_a t}{E t_a}}\ \frac{c}{t} \tag{19}$$

$$\Delta = \frac{1}{2}(\sinh(2\gamma) + \cosh(2\gamma)) \tag{20}$$

$$R_1 = \cosh\gamma \sin\gamma + \sinh\gamma \cos\gamma \tag{21}$$

$$R_2 = \sinh\gamma \cos\gamma - \cosh\gamma \sin\gamma \tag{22}$$

$$k' = \frac{V_o c}{Pt} \tag{23}$$

Hart-Smith [5] modified Goland and Reissner [3] model by conducting an elastic-plastic analysis to the adhesive layer. From the previous models, it is clear that the highest stresses occur at the ends of the adhesive layer, therefore Hart-Smith [5] assumed that the ends of the adhesive layer will deform plastically, while the mid of the adhesive layer will behave elastically as shown in Fig. 8.

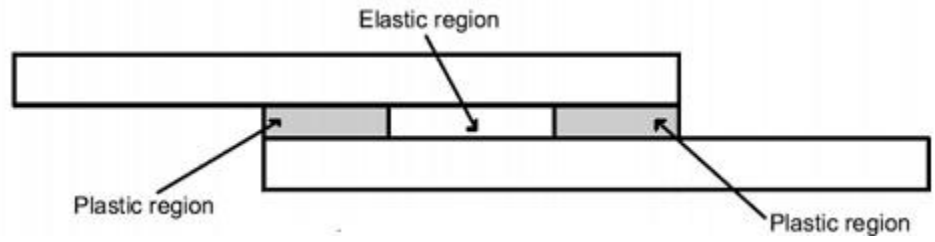

Fig. 8 Adhesive elastic and plastic regions according to hart-smith [7].

Ojalvo and Eidinoff [6] model was similar to Goland and Reissner [3], however Ojalvo and Eidinoff [6] took into account that the shear stress and normal stress vary across the adhesive thickness. There are various models for determining the shear stress and the normal (peel)

stress across the adhesive layer. To better understand each model, Rodriguez [7] plotted the shear stress and the normal (peel) stress distribution for all the analytical models and verified them numerically as shown in both Fig. 9 and Fig. 10. It is evident from Fig. 9 that all the analytical models discussed previously showed that the maximum shear stress is at the ends of the adhesive layer. From Fig. 9, the Volkersen model underestimated the shear stress when compared with the results obtained from the other analytical models and the results obtained numerically from ABAQUS. Moreover, from Fig. 9, it is evident that Hart-Smith (elastic-plastic) has the lowest shear stress at the ends of the adhesive when compared with the other analytical models and the numerical results from ABAQUS. The low shear stress predicted by the Hart-Smith model is due to the elastic-plastic analysis of the adhesive film.

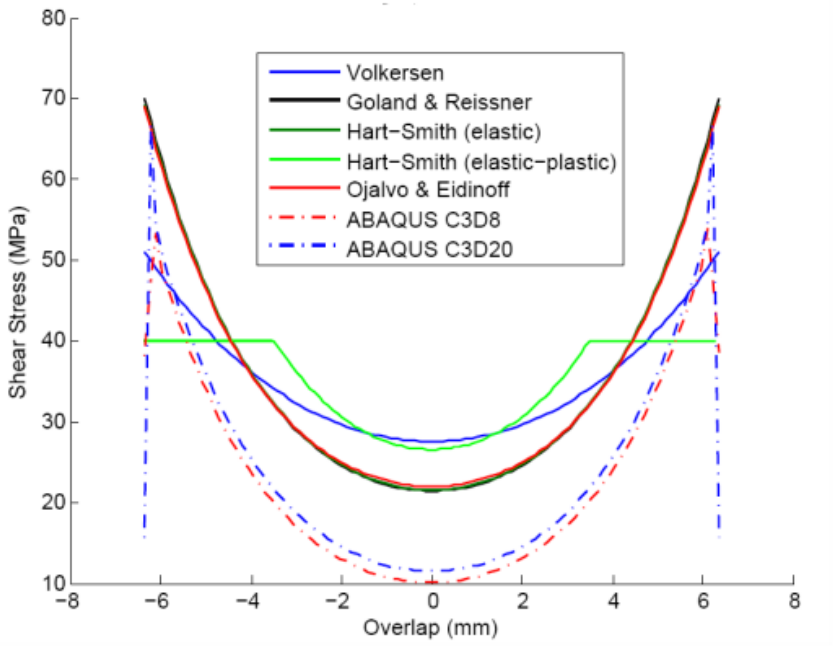

Fig. 9 Shear stress distribution in single lap joint using different models [7].

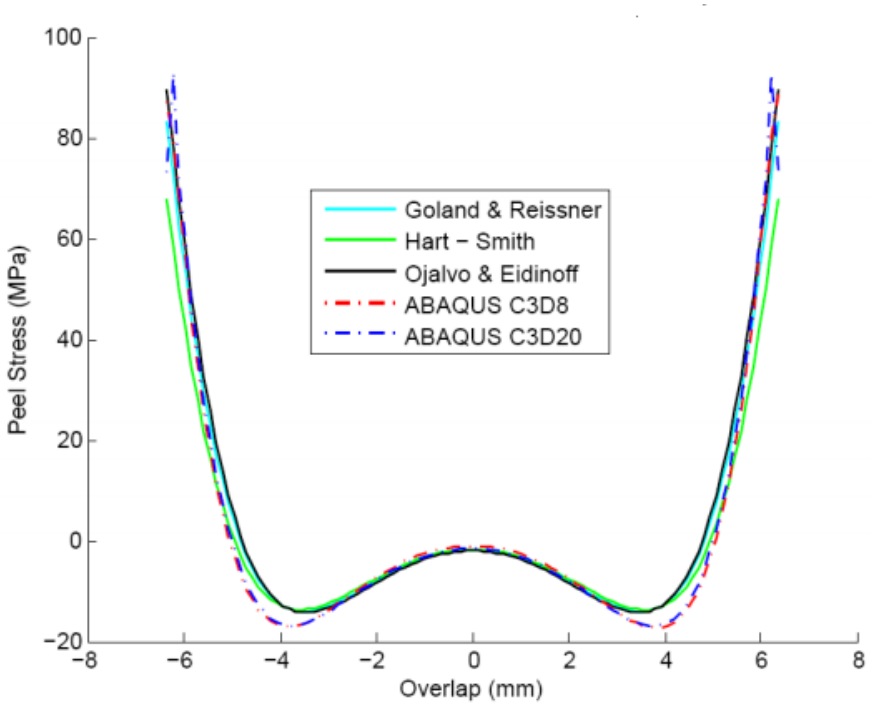

Fig. 10 The peel stress distribution in single lap joint for different analytical models [7].

From Fig. 10, it is obvious that the maximum normal (peel) stress is at the ends of the adhesive layer. Also, the normal stresses predicted by the different analytical models fit perfectly with numerical results from ABAQUS.

I.A.2- Failure modes of single lap joints

According to the standard ASTM D5573 [8], there are seven different failure modes of adhesive bonded fiber reinforced plastic composites single lap joints. These different failure modes are shown in Fig. 11.

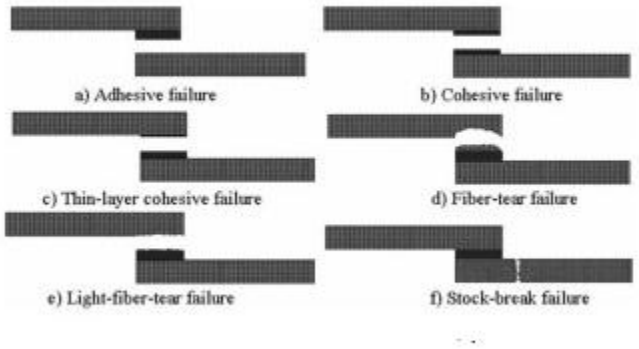

Fig. 11 Different failure modes of fiber reinforced plastic composite single lap joints [9].

The seven different failure modes are:

- Adhesive Failure: As shown in Fig. 11a, the failure occurs at the interface between the adhesive and the adhered, where both the peel stress and the shear stress are the maximum, due to the sharp corner between the adherend and the adhesive. Also this failure mode is called interface failure [9].
- Cohesive Failure: As shown in Fig. 11b, the failure occurs within the adhesive layer itself. Cohesive failure is usually initiated by the presence of manufacturing defects

such as: voids or inclusions that alter the stress field around it and thus a favorable place for cracks to grow.

- Thin layer cohesive failure: This failure mode is the same as cohesive failure mode, however in this mode the failure is usually close to one interface than the other as shown in Fig. 11.c [9].
- Fiber tear failure: In this mode the failure occurs in the matrix of the Fiber reinforced plastic composite adherend [8]. This Failure mode is usually characterized by the appearance fibers on both ruptured surfaces [8].
- Light fiber tear failure: This failure mode is similar to the fiber tear failure mode, however a small chunk of the resin is teared from the adherend [8]. In this failure mode usually small chunks of the resin appear on the top of the adhesive surface with no fibers visible [8].
- Stock-break failure: Failure in this mode happens by the breaking of the fiber reinforced plastic composite adherend [8]. It should be noted that this is the least common failure mode.

Finally, failure can happen in multiple modes.

I.A.3- Defects damage mechanics

Defects usually play an important role in the failure of structural components. The field of damage mechanics is concerned with the irreversible events of the microstructure that leads to the failure of the component [10]. As illustrated in Fig. 12, damage mechanics plays an important role in the durability assessment of a component [10]. Although the process described in Fig. 12 is a reasonable process, it is unrealistic to ignore the effect of defects. These defects play an important role in the initiation and progression of damage leading to the final failure [10]. The amount and the type of Defects usually depend on the manufacturing process. There are different types of manufacturing defects in single lap joints such as: voids, inclusions, disbonds and porosity [11]. It is evident from Fig. 13 that there should be a tradeoff between the cost and performance of the part. For example, a part with a low void content is expected to have a high manufacturing cost. From Fig. 13, it should be noted that the amount of defects within a component could be adjusted to reach the design requirement based on the cost [10].

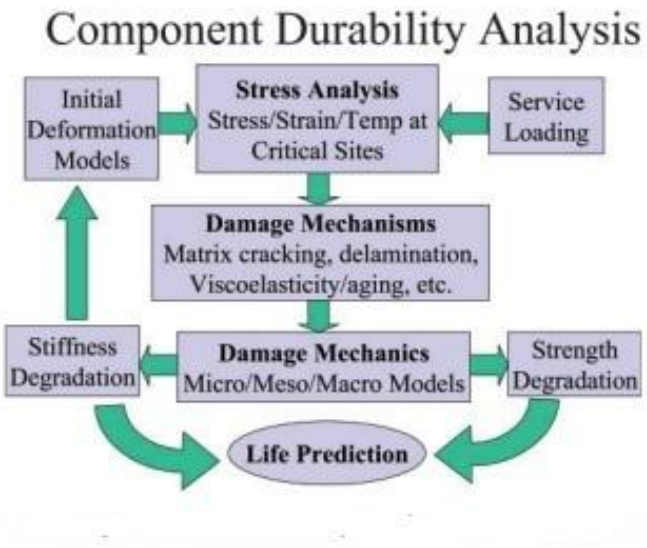

Fig. 12 Damage mechanics for component durability analysis [10].

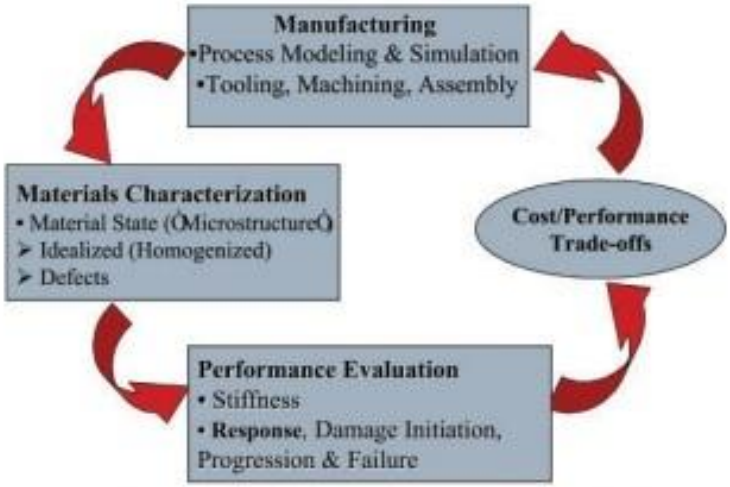

Fig. 13 Iterative process of cost effective manufacturing [10].

I.A.4- Effect of voids in single lap joints

Voids are the most prominent defects in single lap joints. The presence of voids in single lap joints can be attributed to various sources. The most common source is the manufacturing process, for example, during the manufacturing of a single lap joint air might be trapped between the adhesive film and the adherend as shown in Fig. 14a [12]. Another source for the presences of voids in the adhesive film, as shown in Fig. 15, is the presence of volatile impurities that evaporate during the curing of the single lap joint. Also, another source of voids is the entrapment of moisture in the adhesive film due to carelessness while manufacturing the joint. There are numerous studies concerning the effect voids on the mechanical properties of fiber reinforced plastic composites, however there are very few studies about the effect of voids on the mechanical properties of the single lap joints.

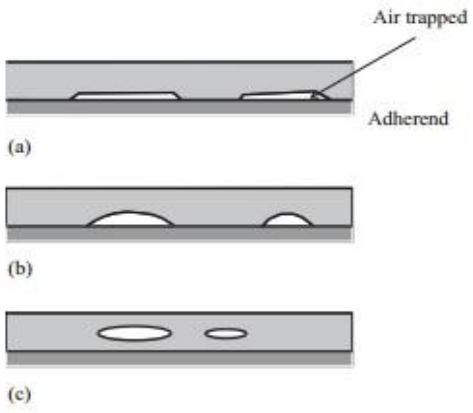

Fig. 14 Air entrapment between adhesive film and adherend : (a) initial entrapment; (b) partial displacement; (c) complete displacement [12].

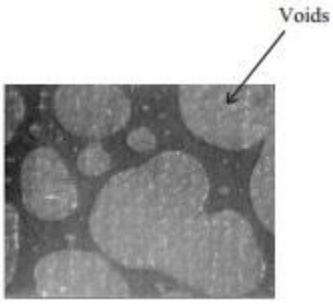

Fig. 15 Voids in an adhesive film [12].

Liu, Ling, Zhang, Wang, and Wu [13] examined the effect of the cure pressure on the void content, the shear strength, the flexural strength and the tensile strength. From Fig. 16, it is obvious that as the cure pressure increases, the flexural strength, the tensile strength and the shear strength increase, however the void content decreases.

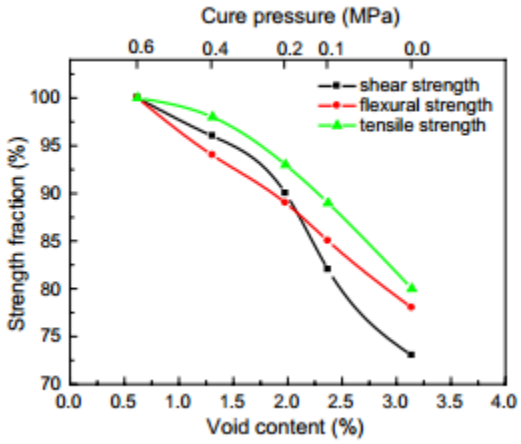

Fig. 16 Effect of the cure pressure on the void content, the flexure strength, the tensile strength and the shear strength [13].

Talreja [10] investigated the effect of voids in resin rich areas between the bundles of a woven fabric laminate on the energy release rate of a double cantilever beam specimen as shown in Fig. 17.

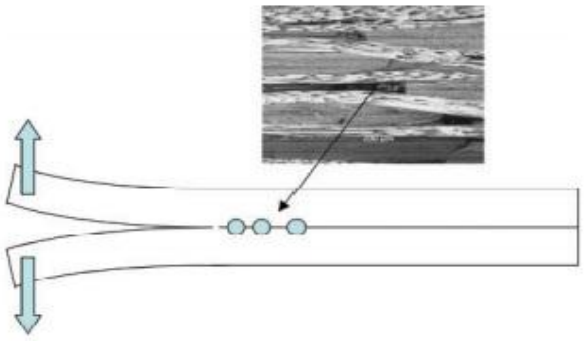

Fig. 17 Voids in resin rich areas between bundles in woven fabric laminate and DCB specimen representation of crack growth in presence of voids [10].

From Fig. 18 and Fig. 19, It can be concluded that the presence of voids in resin rich areas increases the Mode I energy release rate, which is the driving force for the crack growth.

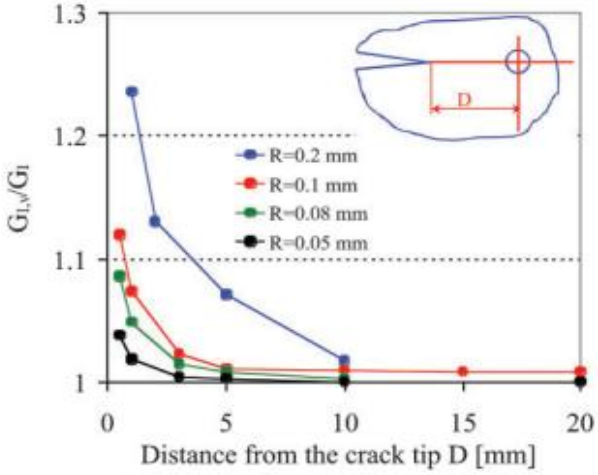

Fig. 18 Effect of the void radius and the distance from the crack tip on the energy release rate [10].

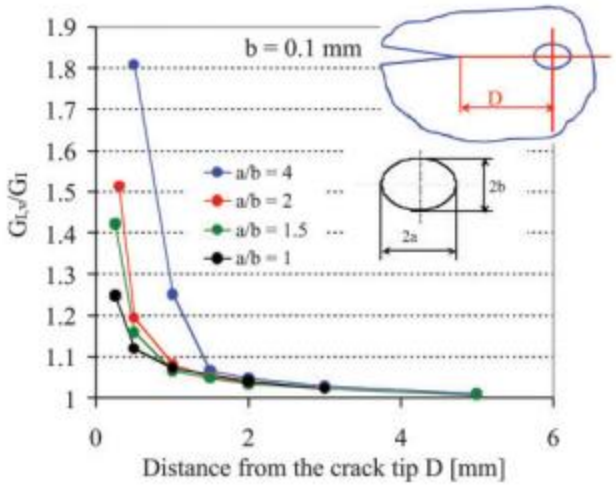

Fig. 19 Effect of the void shape and the distance from the crack tip on the energy release rate [10].

Also from Fig. 18, It is clear that increasing the radius of the void increases the driving force for the crack growth , which means that the presence of the void makes it easier for the crack to grow.It can be inferred from Fig. 19 that the elliptical voids increase the driving force for the crack growth when compared with the circular voids. Moreover from Fig. 18 and Fig. 19, It can be concluded that as distance between the void and the crack tip increases, the Mode I energy release rate for the void case is approximately the same as the non void case due to saint venant principle. There are very few studies conducted on the effect of voids in adhesive films and most of these studies are conducted on the strength of single lap joints without taking the effect of defects into consideration. For example, Shahin and Taheri investigated [14] the effect of the adherends thickness in unbalanced joint on the energy release rate. Also, Rossettos, Lin and Hashemi [15] examined the effect of voids on the shear stress and the normal stress distribution in single lap joints. This study is one among the few studies conducted on the effect of voids in adhesive films of single lap joints [15]. The void

in this study is represented as a gap or a recess in the adhesive with sharp corners as shown in Fig. 20 which is not practacial, as the void shape and size play an important role in stress distrbution as shown Fig. 18 and Fig. 19 [10].

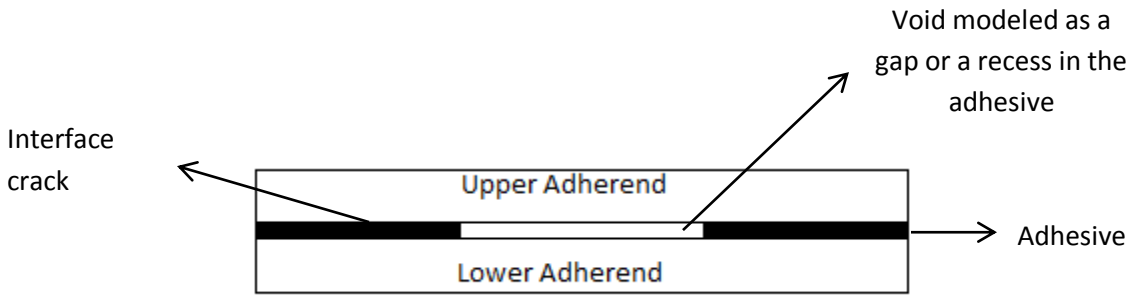

Fig. 20 Void in the single lap joint [16].

Chadegani and Batra [16] investigated the effect of a void on the energy release rate of an interface crack. The void was modeled as a gap, as shown in Fig. 20, with no consideration to the void shape and size which is not practical, because Talreja [10] showed that the void shape and the void radius do have an influence on the energy release rate. The kinking of an interface crack between two elastic layers was studied before by Suo and Hutchinson [17]. The effect of of the void radius, the void shape and the void distance from an interface crack on the energy release rate was not studied before in a single lap Joint. Also , the effect of a void on the kinking of a crack from the interface into the adhesive in single lap joints was not studied before, therefore it is essential to understand how the void shape or radius could lead a crack to kink from the interface into the adhesive.

I.B- Problem statement

The main objective is to understand how manufacturing defects -voids- could lead an interface crack to kink into the adhesive film of a single lap joint. A pre crack will be embedded in the interface, because it is the region where both the shear stress and the normal stress are the maximum. Since it is an interface crack, the crack is expected to grow in mixed mode. The effect of different void parameters will be investigated. These parameters are the distance of the void from the crack tip, the void radius and the void shape. It is very hard and expensive to understand the effect of the void parameters experimentally; therefore it is better to use numerical analysis to understand their effect. Only one void will be taken into consideration, because previous studies have shown that the first void ahead of the crack tip is the most critical one [18]. The energy release rate will be calculated using the revised virtual crack closure (RVCCT) technique. The revised virtual crack closure technique (RVCCT) is a very powerful tool, because each fracture mode can be calculated separately -Mode I and Mode II -. The total driving force is computed from the revised virtual crack closure technique (RVCCT) by adding Mode I and Mode II then the results are justified by the J-integral method. The interface crack is assumed to grow a certain distance at different angles. The angles vary from 0-90 degrees with an increment of 10 degrees. The energy release rate is calculated for each angle with and without the void to understand how the void changes the energy release rate. After computing the energy release rate at different kink angles, the crack is expected to grow in the direction that maximizes the energy.

CHAPTER II

NUMERICAL STUDY OF THE INTERFACE CRACK WITHOUT THE VOID

In the following chapter, the energy release rate of an interface crack in a single lap joint without the presence of a void is investigated. A two dimensional plane strain geometriclly nonlinear finite elements model is develop to study the behaviour of the cracked single lap joint. The geometric nonlinear finite elements mesh is shown in Fig. 23. The total energy release rate is calculated by the revised virtual crack closure technique (RVCCT) and the J- integral method.

II.A- Geometry of the studied single lap joint

Fig. 21 shows an illsutration of the single lap joint that will be studied in this section. For the model verification purpose, the single lap joint is made of two alumnium adherends and a thin adhesive film as shown in Fig. 21. The length of the upper adherend and the lower adherend without the adhesive overlap is "l" and its length is 125mm. Also From Fig. 21, the thickness of the upper adherend and the lower adherend is "t" and it is equal to 1.5mm. Moreover from Fig. 21, the adhesive film thickness is "t_a" and it is equal to 0.3mm. In addition, from Fig. 21, the adhesive film length is "$2c$" , which is 50mm. Finally from Fig. 21, the interface crack length is denoted by "a" and it is equal to 25mm. The material properties of the adherends and the adhesive film are shown in Table .1

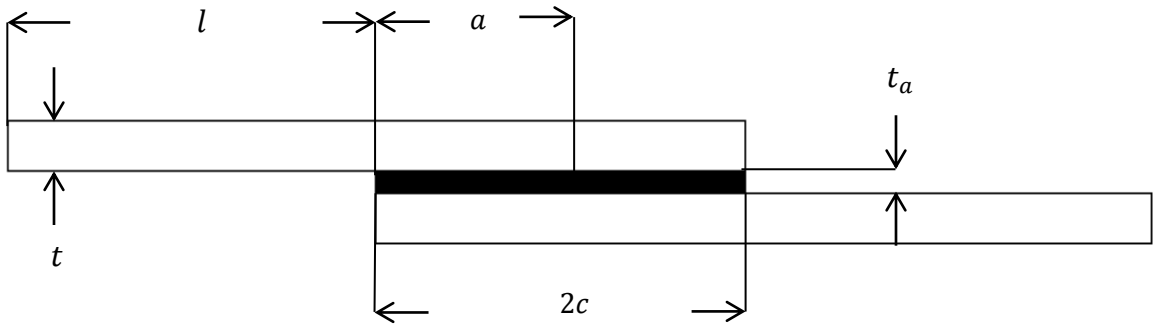

Fig. 21 Single lap joint illustration.

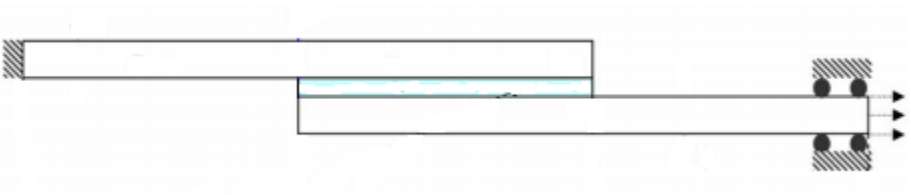

Fig. 22 Boundary condition [19].

The boundary conditions that are used during the analysis are shown in Fig. 22. The boundary conditions are chosen such that they induce a bending moment within the the single lap joint. The single lap joint is fixed firmly at left end as shown in Fig. 22 [19]. Also, a force boundary condition is applied at the right end. It should also be noted that the right end of the adherend is restrained in the veritcal direction as shown in Fig. 22. The material properties used in this chapter were adopted from [20] and [21].

Table. 1 Material properties [20], [21].

	Youngs Modulus (GPA)	**Poisson's Ration**
Adherend (Aluminum)	69	0.33
Adhesive (Epoxy)	2.07	0.345

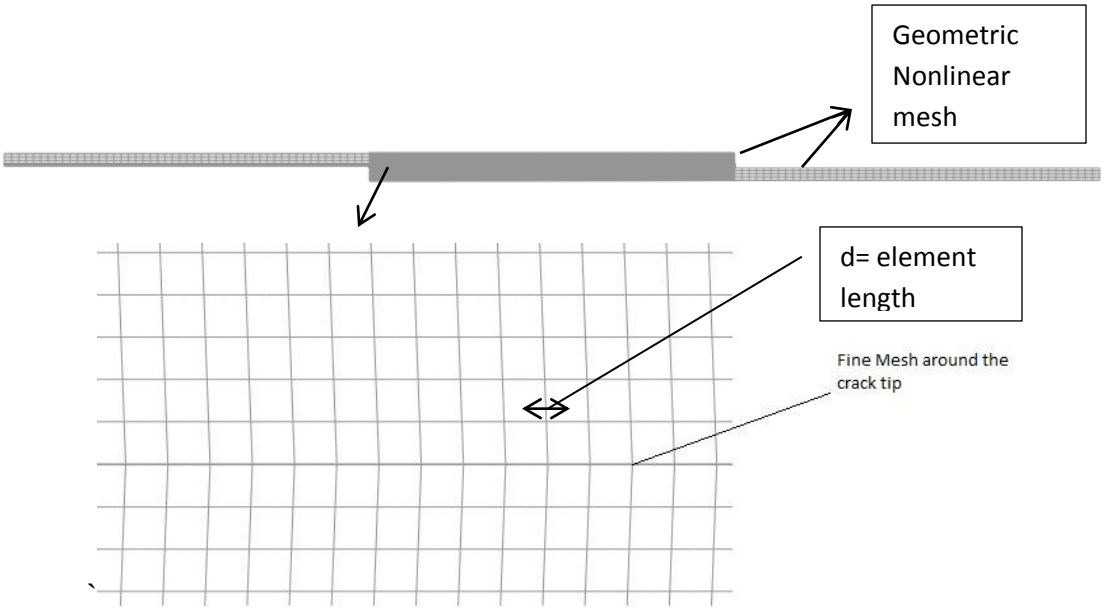

Fig. 23 Geometric non linear finite elements mesh.

The energy release rate was computed using the revised virtual crack closure technique (RVCCT), which is a modifcation of the virtual crack closure technique (VCCT). The virtual crack closure technique (VCCT) is a linear elastic fracture mechanics technique that was developed by Rybicki [22] to compute the energy release rate. The virtual crack closure technique (VCCT) is based on the the assumption that the amount of energy required to open a crack a certain distance is equal to the amount of energy required to close the same crack

the same distance [22]. Mode I and Mode II energy release rates can be calculated using the following equations :

$$G_I = -\frac{1}{2d}\left(-Z_i(W_l - W_l{}^*) + Z_j(W_m - W_m{}^*)\right) \tag{24}$$

$$G_{II} = -\frac{1}{2d}\left(-X_i(U_l - U_l{}^*) + X_j(U_m - U_m{}^*)\right) \tag{25}$$

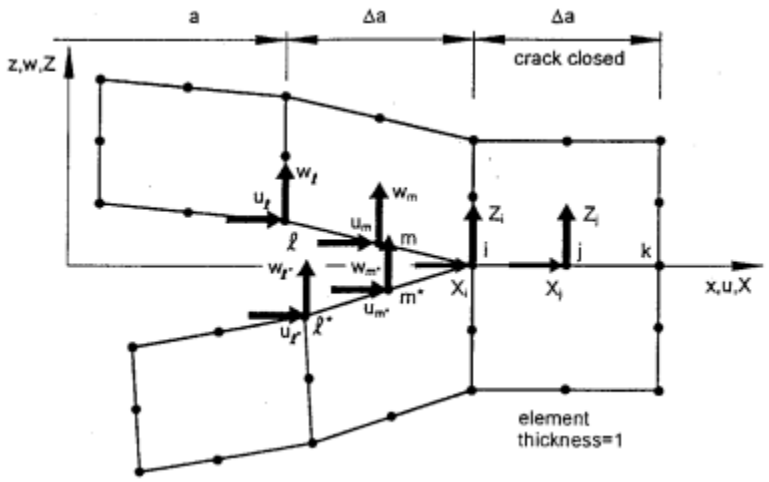

Fig. 24 Virtual crack closure technique method [23].

The energy release rates calculated by equations (24) and (25) are based on an eight noded element, where Z_i and Z_j represent the nodal forces in vertical directions at nodes i and j. Also, X_i and X_j represent the nodal forces in horizontal direction for nodes i and j respectively. Moreover, From Fig. 24 W_l, $W_l{}^*$, W_m and $W_m{}^*$ are the vertical displacements at nodes l, l^*, m and m^* respectively. In addition, from Fig. 24. U_l, $U_l{}^*$, U_m and $U_m{}^*$ are the horizontal displacements at nodes l, l^*, m and m^* respectively [23]. For more accurate

calculations of the energy release rates, a very fine square uniform mesh is preferred around the crack tip. The element size ”d” is taken to be 0.01 mm around the crack tip.

II.B- Revised virtual crack closure technique

Since the crack is an interface crack, the stresses around the crack tip are expected to oscillate [24] i.e: the stresses have positive and negative values. As a result of these osciallating stresses, the values of Mode I and Mode II energy release rates calculated by the virtual crack closure technique (VCCT) might be negative, which is not practical. For unsymmetrical cracks, the revised virtual crack closure technique (RVCCT) is more powerful than the virtual crack closure technique (VCCT).

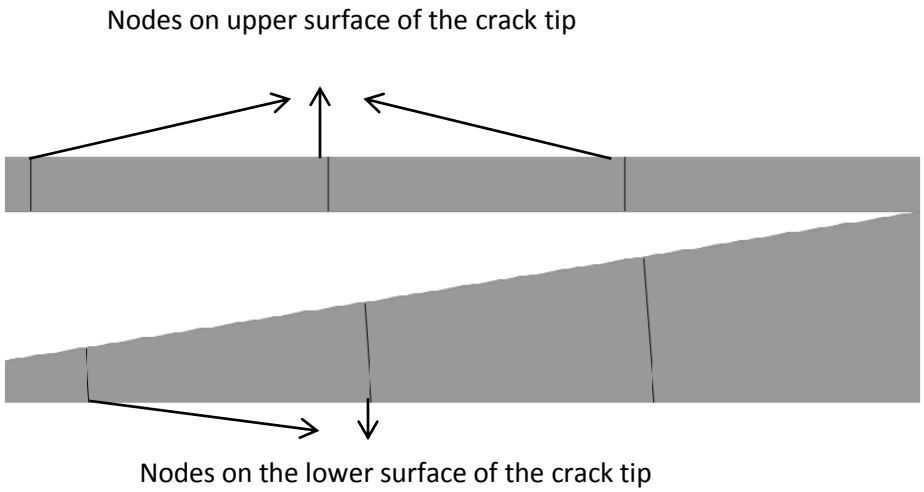

Fig. 25 Unsymmetrical crack.

For unsymmetrical cracks with elements of the same size, the nodes on the upper surface of the crack tip will never be coincident with the nodes on the lower surface of the crack tip as

shown in Fig. 25 and Fig. 26, therefore the accuarcy of the results obtained by virtual crack closure technique (VCCT) will be compromised. The Revised virtual crack closure technique (RVCCT) depends on the stiffness of the mesh and hence it gives more accurate results when compared with the virtual crack closure technique (VCCT) [25]. The different fracture modes for the revised crack closure technique (RVCCT), which are Mode I and Mode II can be obtained from the following equations:

$$G_I = \frac{1}{2d}\left(\frac{\Delta W_c{}^2}{f_{zz}}\right) \tag{26}$$

$$G_{II} = \frac{1}{2df_{zz}}\left(\frac{(f_{zz}\Delta U_c - f_{xz}\Delta W_c)^2}{f_{zz}f_{xx} - f_{xz}{}^2}\right) \tag{27}$$

$$\Delta W_c = W_{c2} - W_{c1} \tag{28}$$

$$\Delta U_c = U_{c2} - U_{c1} \tag{29}$$

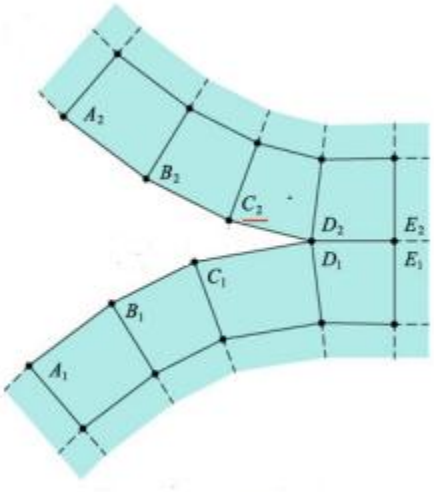

Fig. 26 Unsymmetrical crack for illustration of revised virtual crack closure technique (RVCCT) [25].

$W_{c2}$and W_{c1} are the vertical displacements of nodes c_2 and c_1 respectiveley. Also $U_{c2}$and U_{c1} are the horizontal displacements of nodes c_2 and c_1 resepctiveley. f_{xx} , f_{xz} , f_{zx} and f_{zz} are called the flexibilty constanst and they are mesh dependent constants [25]. These flexibilty constants are calculated by applying unit loads at nodes c_2 and c_1.

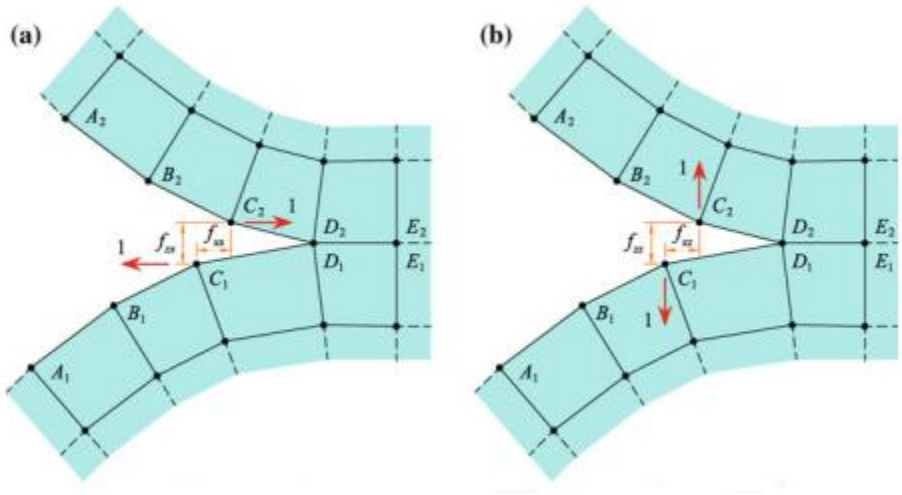

Fig. 27 Computations of flexibility coefficents : a) unit force in the x-direction b) unit force in the y-direction [25].

For example, to compute f_{xx} and f_{zx} a positive unit load is applied to node c_2 in the positive x- direction and a negative unit load is applied to node c_1 in the negative x-direction as shown in Fig. 27a. The values of f_{xx} and f_{zx} can be calculated from the following equations [25]:

$$f_{xx} = U_{c2} - U_{c1} \tag{30}$$

$$f_{zx} = W_{c2} - W_{c1} \tag{31}$$

Also, to calculate f_{xz} and f_{zz} a positive unit load in applied to node c_2 in the positive y-direction and a negative unit load is applied to node c_1 in the negative y-direction as shown in Fig. 27b. The values of f_{xz} and f_{zz} can be calculated from the following equations:

$$f_{xz} = U_{c2} - U_{c1} \tag{32}$$

$$f_{zz} = W_{c2} - W_{c1} \tag{33}$$

II.C- Finite elements model validation

In order to gain confidence in the finite elements model, the results of the total energy release rate obtained by the revised virtual crack closure technique (RVCCT) will be compared to the results obtained by analaytical model. The analytical model is developed by Kafkalidis and Thouless [26] based on Suo and Hutchinson interface crack problem [17]. The total energy release rate derived by Kafkalidis and Thouless [26] is the following:

$$G_T = \frac{P^2}{2Et} + \frac{6{M_o}^2}{Et^3} - \left[\frac{P^2}{4Et} - \frac{12(M_o - kPt)^2}{16Et^3}\right] \tag{34}$$

According to Kafkalidis and Thouless [26], equation (34) is only valid if the crack length "a" in much larger the adherend thickness "t". In the finite elements model shown in Fig. 23, in page 23, the crack length "a" is 25mm and the adherend thickness "t" is 1.5mm, therefore the crack length is much larger than the adherend thickness as required by equation (34). The results obtianed by revised virtual crack closure (RVCCT) and the J- integral will be verified with the results obtained by equation (34). Moreover, Fig. 28 Shows the shape of the single lap joint after deformation. Table. 2 shows the values of the total energy release

rates obtained by different methods. Also, Table. 3 shows the percentage error between the different methods used to calculate the total energy release rate. For example, it is clear from Table. 3 that the percentage error between the J-integral method and equation (34) is around 7.5%. Also, the pecentage error between the J- integral and revised crack closure technique (RVCCT) is around 10% and the percentage error betweeen revised crack closure technique (RVCCT) and equation (34) is around 2.5%.

Table. 2 Total energy release rate obtained by different methods.

Load (N/mm)	Kafkalidis and Thouless Model	RVCCT	J-integral
1	0.014	0.013	0.015
2	0.054	0.054	0.059
4	0.219	0.215	0.236
6	0.496	0.483	0.531
10	1.374	1.345	1.476
20	5.495	5.380	5.905
40	21.981	21.471	23.619
60	49.456	48.336	53.142
80	87.922	86.0151	94.475
100	137.378	134.503	147.617
120	197.825	194.228	212.338
140	269.260	263.309	289.329
150	309.100	302.632	332.138

Table. 3 Percentage error between the different total energy release rates methods.

% error (J-integral& Thouless model)	% error(J-integral&RVCCT)	% error(Thouless model&RVCCT)
7.3	9.6	2.1
7.5	9.7	2.1
7.5	10.0	2.4
7.5	9.9	2.3
7.5	9.7	2.1
7.5	9.7	2.1
7.5	10.0	2.4
7.5	9.9	2.3
7.5	9.8	2.2
7.5	9.7	2.1
7.3	9.3	1.9
7.5	9.9	2.26
7.5	9.7	2.14

Fig. 28 Deformed shape of a single lap joint with and interface crack.

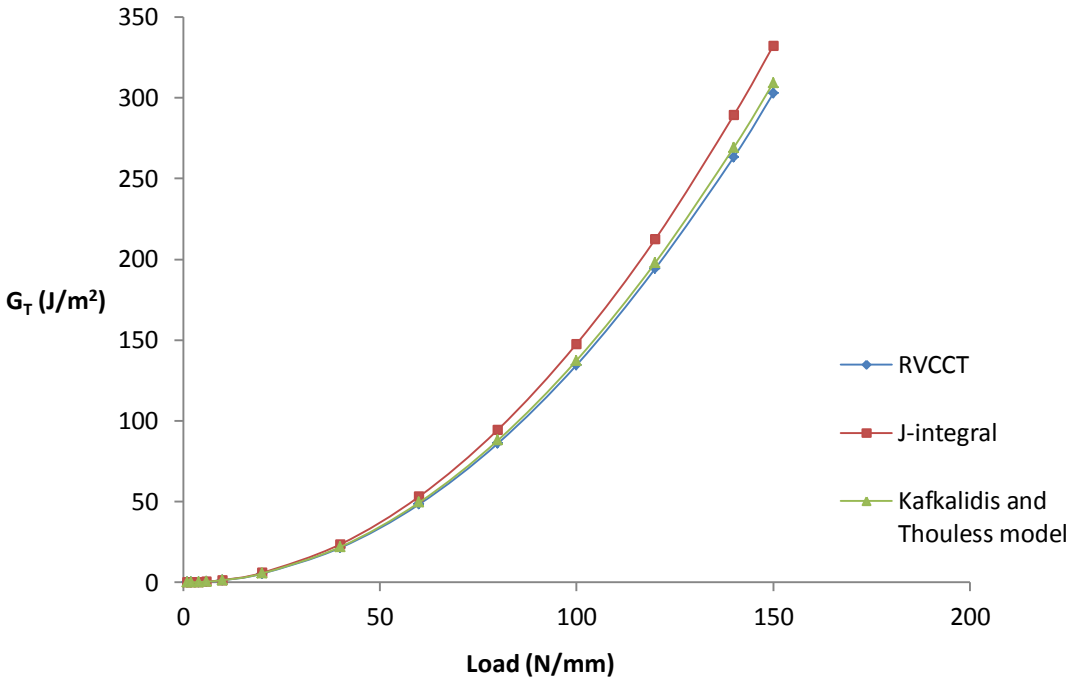

Fig. 29 Total energy release rates by different techniques.

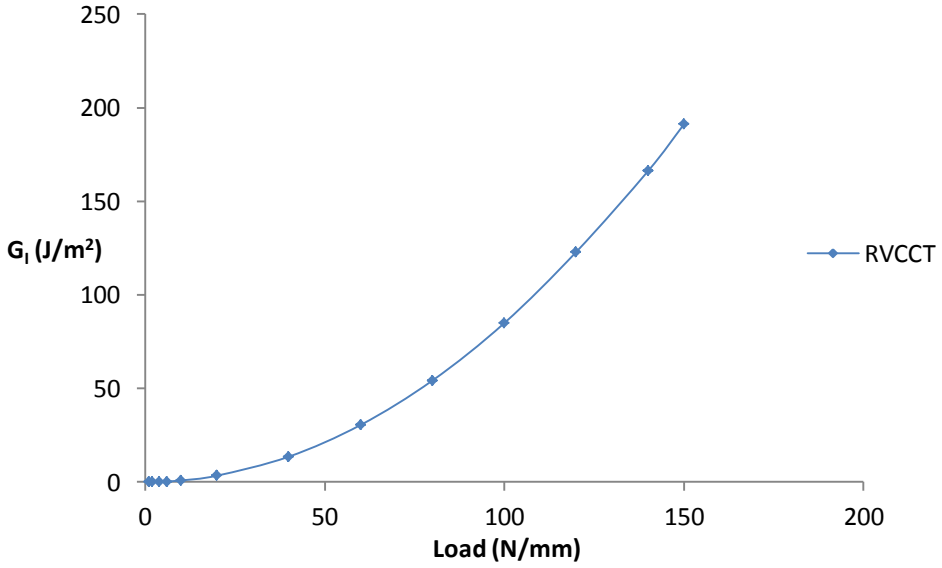

Fig. 30 Mode I energy release rate.

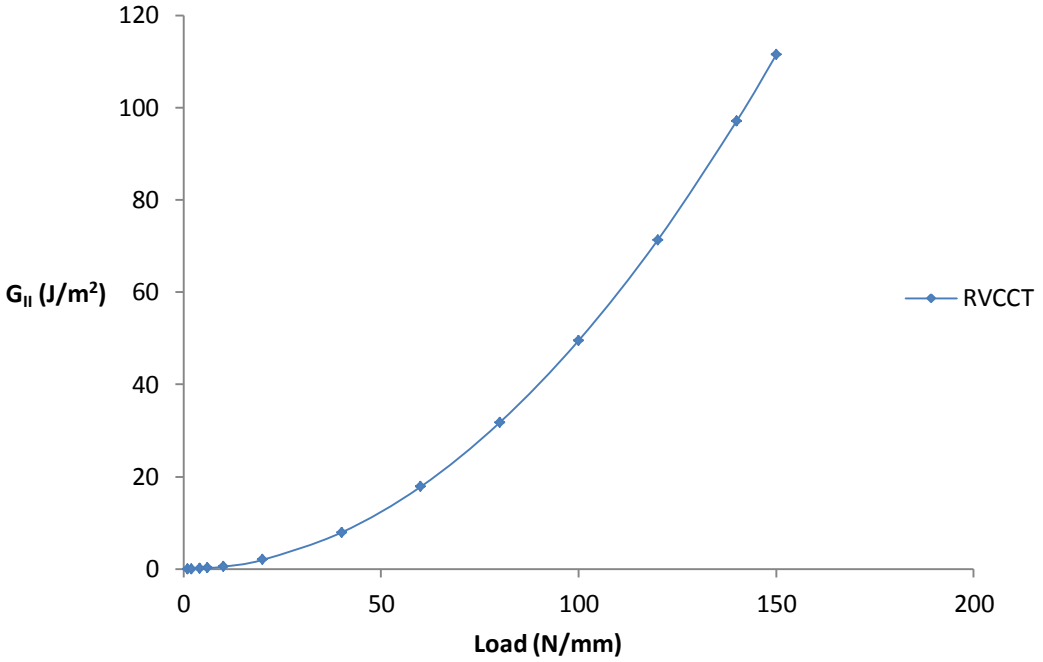

Fig. 31 Mode II energy release rate.

It is obvious from Fig. 29 that by increasing the load, the total energy release rate increases. Also, the results obtained by the revised virtual crack closure technique (RVCCT) from the finite elements model are approximately the same as the results obtained from equation (34) and the J- integral method, which justifies the finite elements model. Fig. 30 and Fig. 31 show that as the load increases, Mode I and Mode II energy release rates increase. Finally from Fig. 30 and Fig. 31, It is evident that Mode I contributes more than Mode II in total energy release rate.

CHAPTER III

PARAMETRIC STUDY OF VOIDS AND CRACK KINKING

In this chapter the effect of voids on the crack kinking process will be studied. A two dimensional plane strain geometrically nonlinear finite elements model is used, however the void is incorporated in the model to study its effect on the energy release rate.

III.A- Geometery of the studied single lap joint

Fig. 32 shows the geometry of studied single lap joint with the void incoporated in it. The length of the upper adherend and the lower adherend without the adhesive bond is "l" and it is equal to 50mm. The thickness of the upper adherend and the lower adherend is "t" and it is 1.5mm The crack length is denoted by "a" and it is 12.5mm. Also, the adhesive bond length is donoted by "$2c$" and it is 50mm. Finally, the adhesive bond thickness is denoted by "t_a" and it is 0.3mm. The material properties that are used in the analyais are shown in Table. 4. The material properties were adopted from [21] and [27]. Also, Fig. 33 shows a representation of the geometric non linear finite elements mesh. A Force of 150 N/mm is used in the parameteric studies in the coming sections, while the other boundary conditions are the same as the non void case.

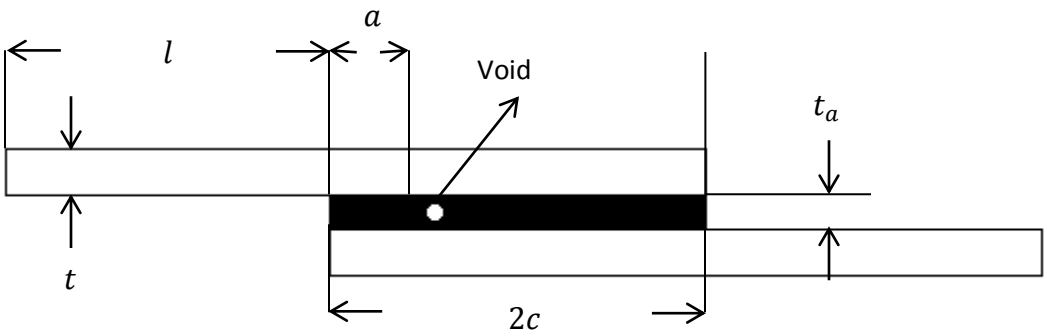

Fig. 32 Single lap joint schematic with void.

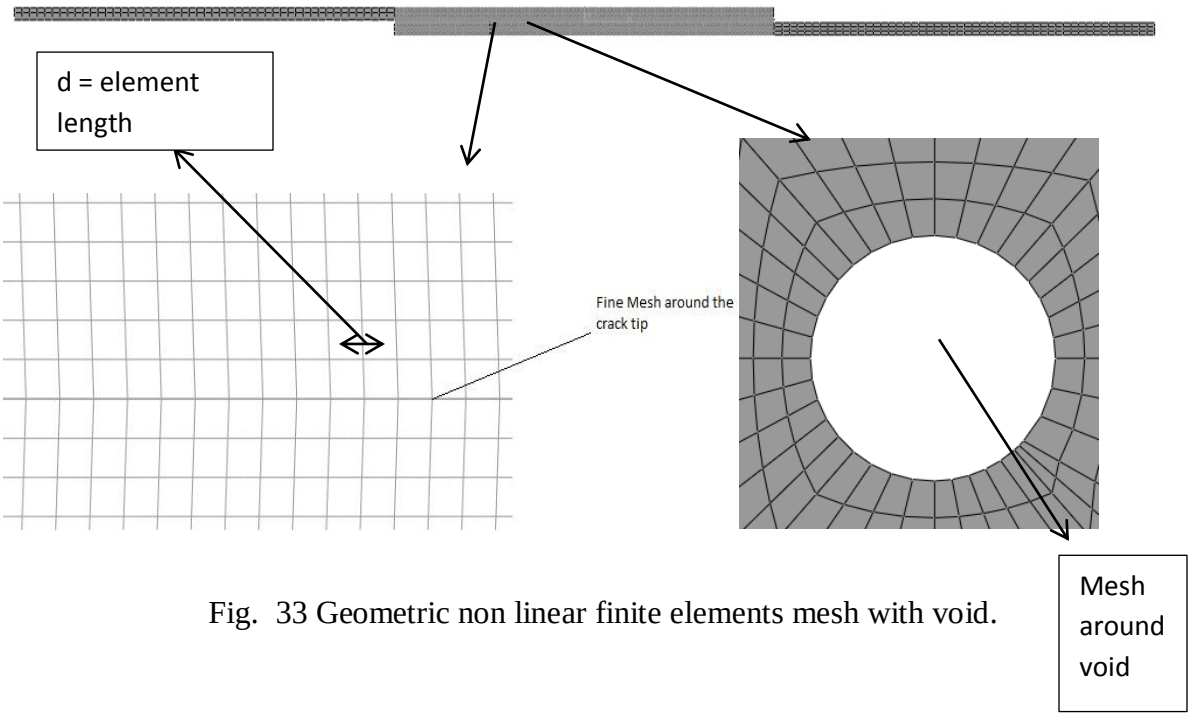

Fig. 33 Geometric non linear finite elements mesh with void.

Table. 4 Material properties of the single lap joints in GPA [21],[27].

Material	**E11**	**E22=E33**	**ν12= ν13**	**ν23**	**G12= G13**	**G23**
Adherend	130	11.2	0.306	0.48	5.3	3.78
Adhesive	2.07	2.07	0.345	0.345	0.769	0.769

III.B- Void modelling

The effect of the void distance from the crack tip, the void radius and the void shape will be studied in this section. There are very few studies that report the size and the shape of voids detected in the adhesive film of single lap joints. Hadj-Ahmed [28] reported voids of radius 0.025mm approximately in the adhesive film of a single lap joint as show in Fig. 34.

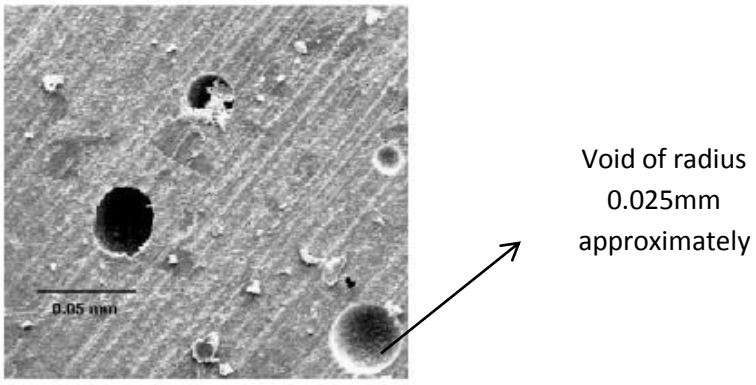

Fig. 34 Voids in an adhesive film.

III.C- Effect of the void location on the energy release rate

In this study, the effect of the horizontal void location on the crack kinking is taken in consideration. The intereface crack is assumed to extend a small increment of 0.1mm at different angles. These angles range from 0 to 90 degrees with an increment of 10 degrees as shown in Fig. 35. For each path or angle, Mode I and Mode II are calucated using the revised virtual crack closure technique (RVCCT) and the total energy release rate is caluclated by adding Mode I and Mode II then the results wil be justified by the J – integral method. The horizontal distance between the crack tip and the void is denoted by “d1”. A void of radius

0.03mm is used in the analysis, which is similar to the radius of the void reported by Hadj-Ahmed [28]. Fig. 36, Fig. 37 and Fig. 38 show Mode I energy release rate at different kinking angles for different void locations. From these figures, as the kinking angle increases, mode I energy release rate decreases, which means that the favourable angle for the crack growth even with the presence of the void is the interface.

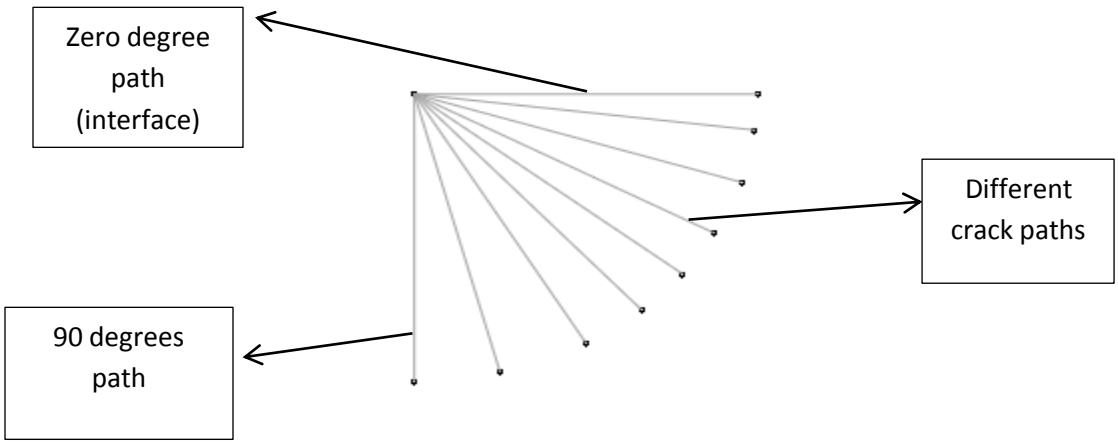

Fig. 35 Different crack paths at different angles.

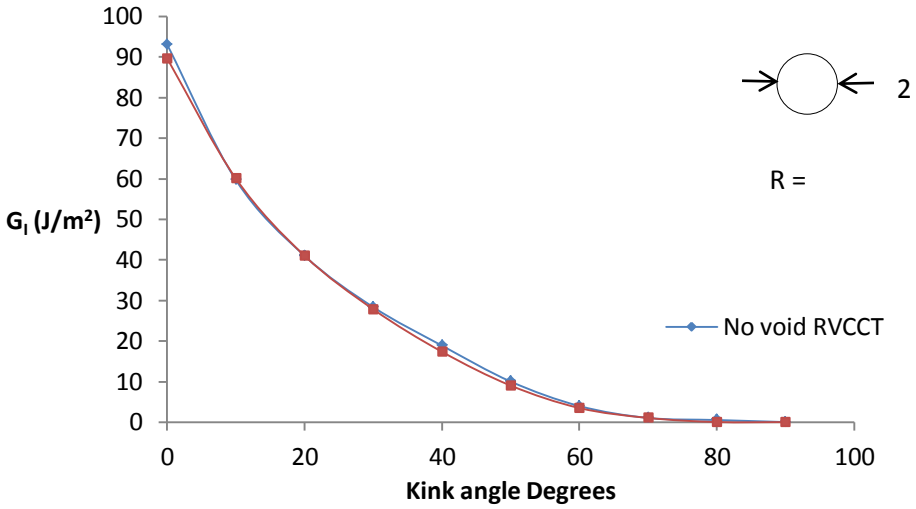

Fig. 36 Mode I energy release.

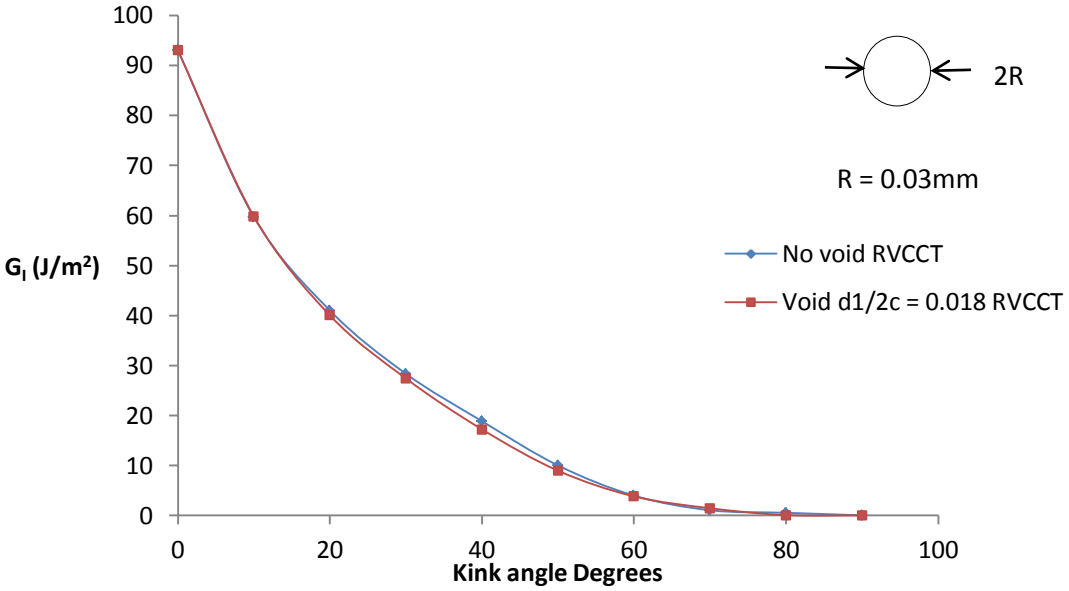

Fig. 37 Mode I energy release rate.

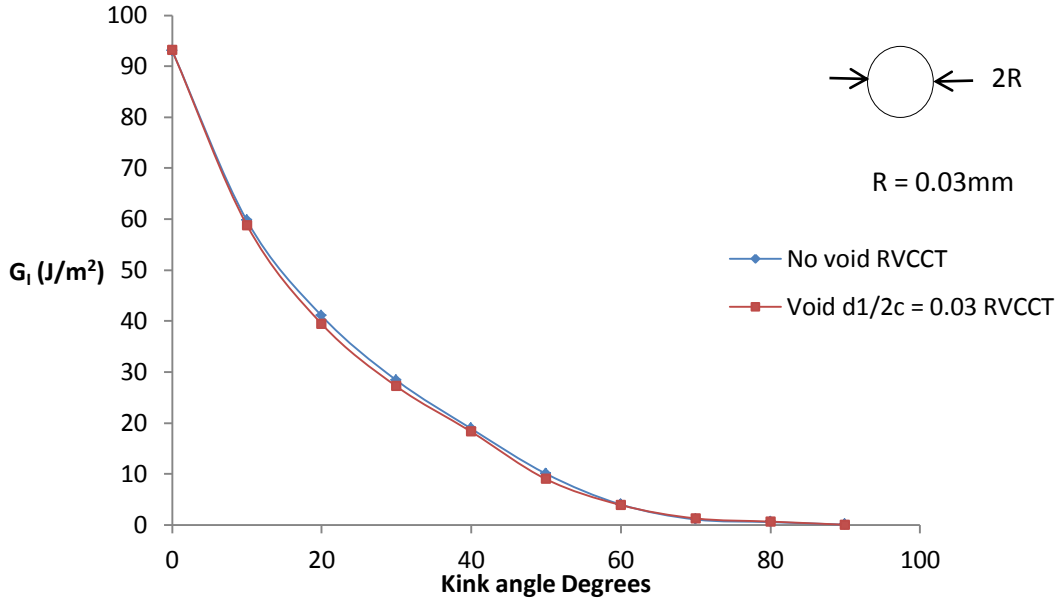

Fig. 38 Mode I energy release rate.

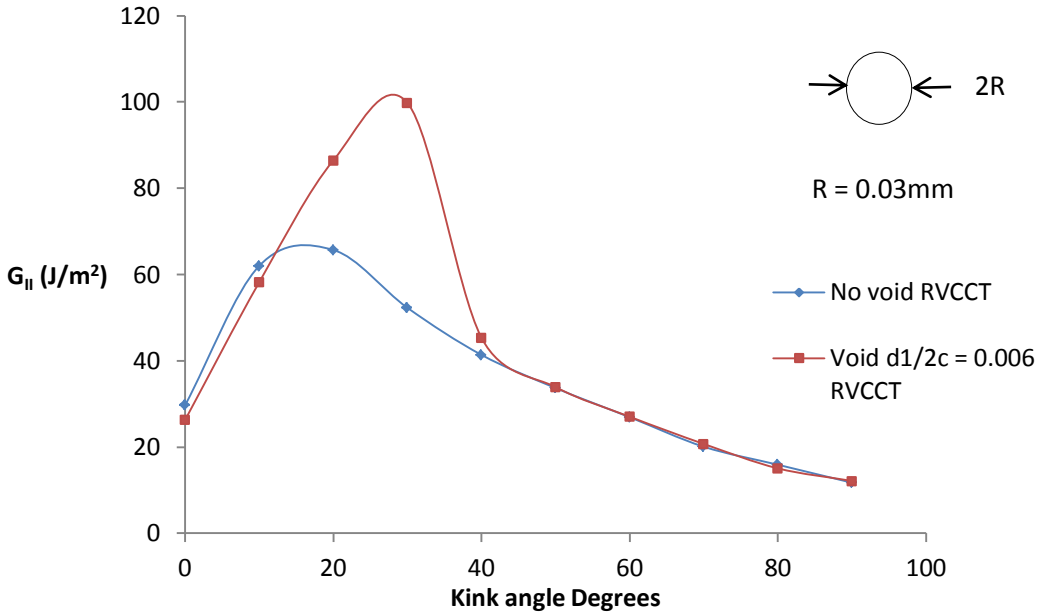

Fig. 39 Mode II energy release rate.

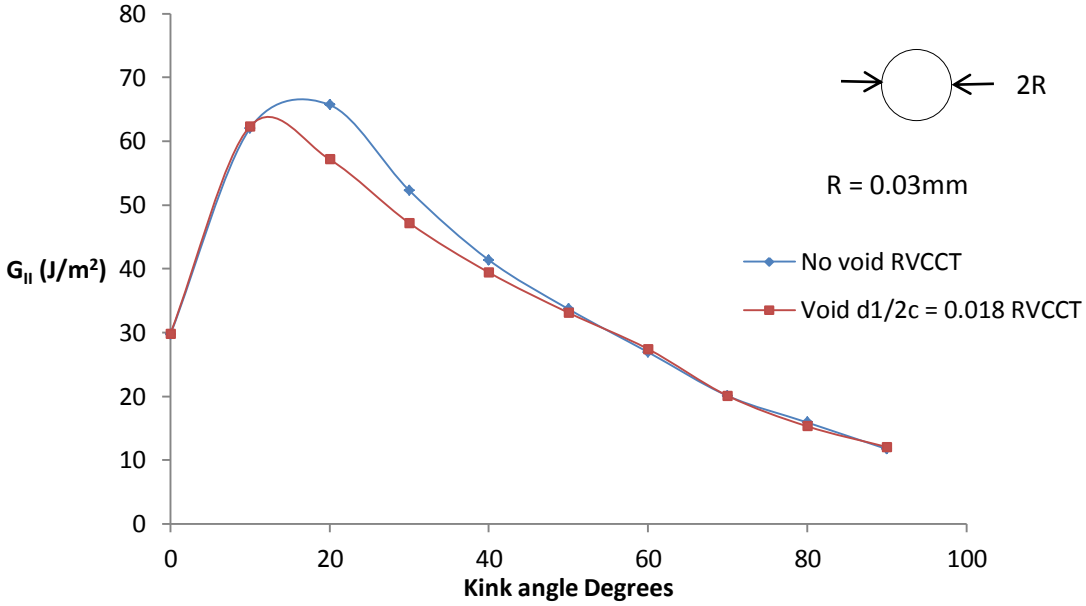

Fig. 40 Mode II energy release rate.

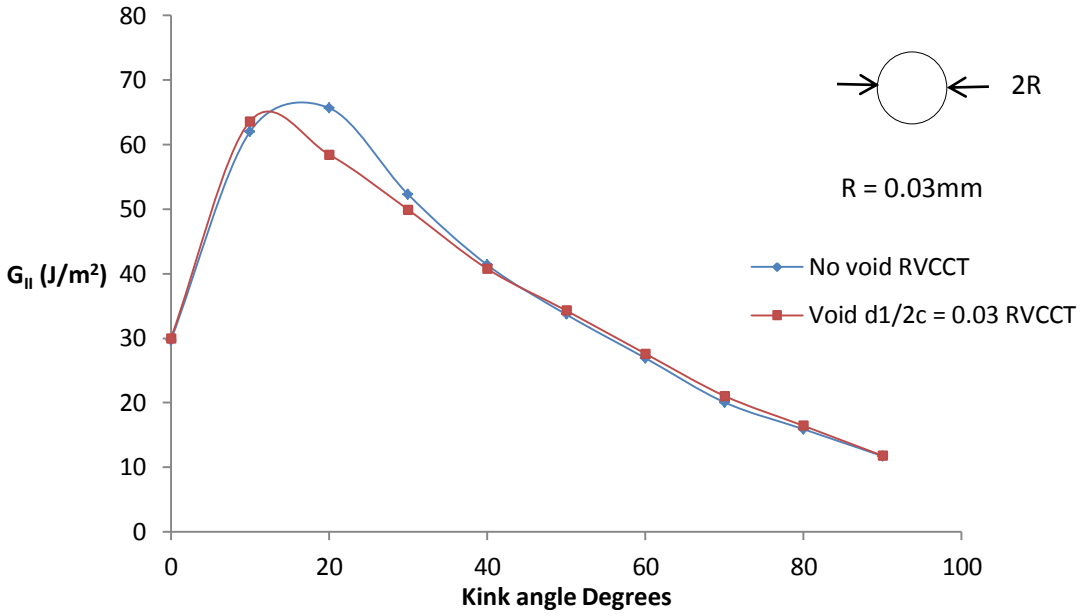

Fig. 41 Mode II energy release rate.

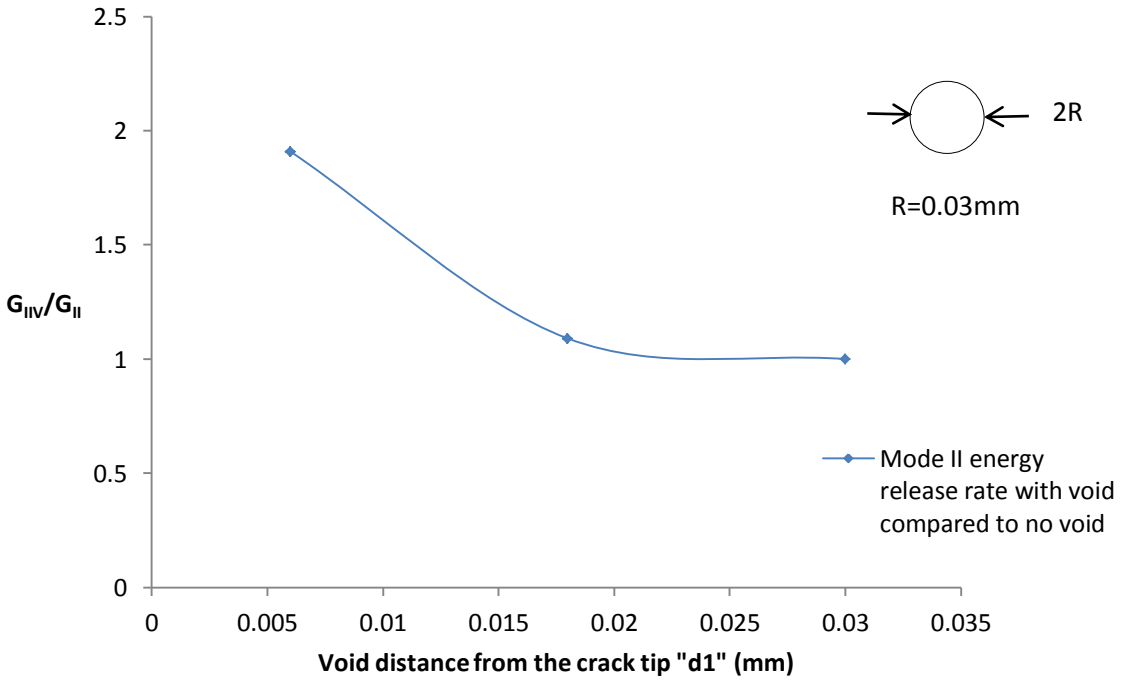

Fig. 42 Ratio of the maximum value of Mode II in Fig. 39, Fig. 40 and Fig. 41with ratio to the corresponding non void values.

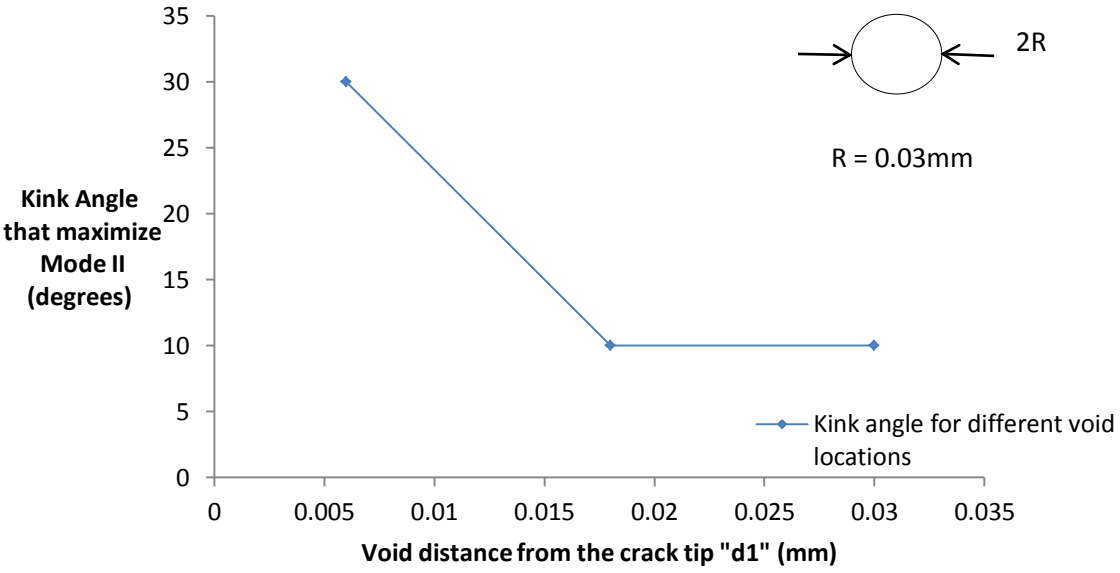

Fig. 43 Angles at which Mode II is maximum in Fig. 39, Fig. 40 and Fig. 41 and the corresponding distance of the void from the crack tip.

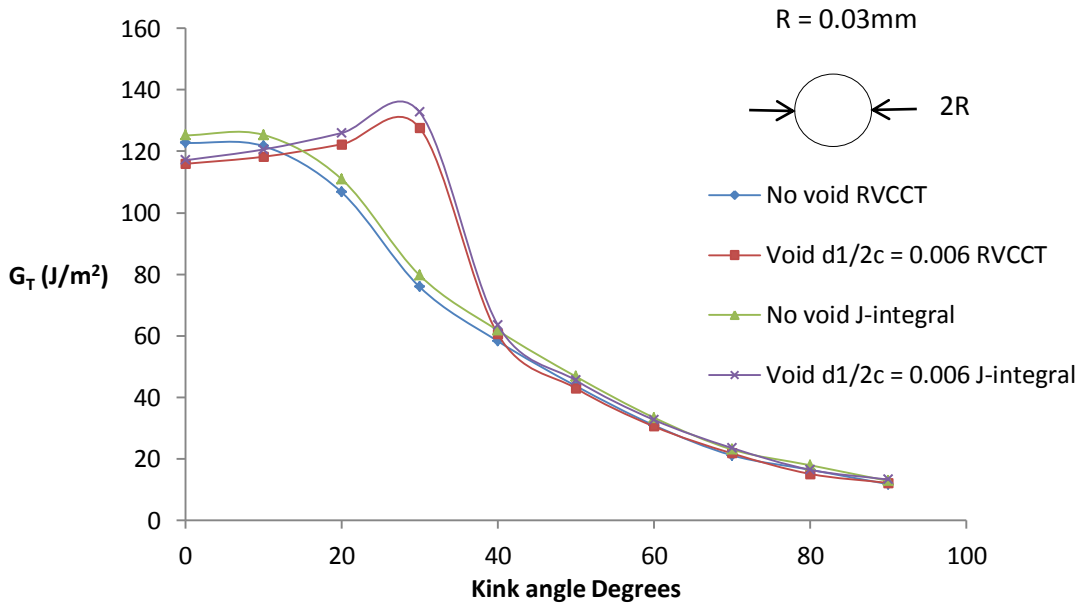

Fig. 44 Total energy release rate.

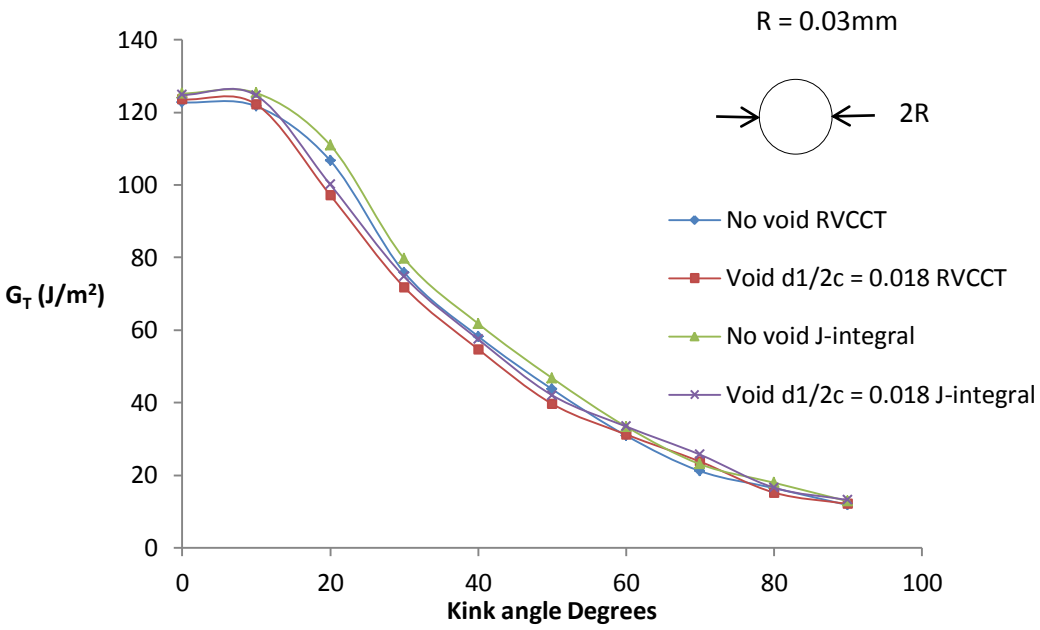

Fig. 45 Total energy release rate.

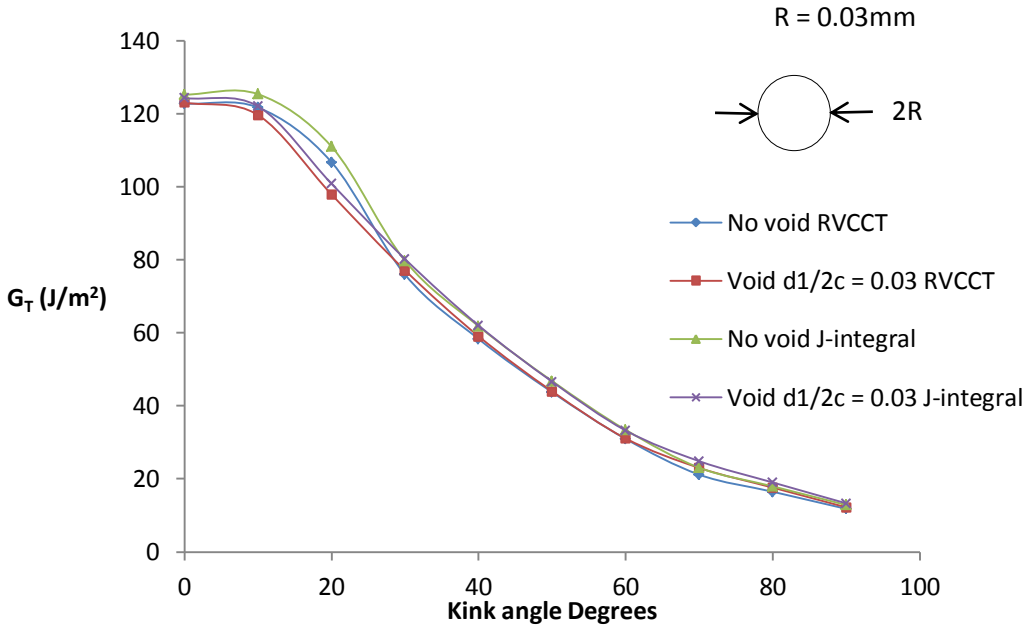

Fig. 46 Total energy release rate.

From Fig. 36 in page 36, Fig. 37 and Fig. 38 in page 37, the presence of a void regardless of its position did not affect the behaviour of Mode I energy release rate. Fig. 40 in page 38 and Fig. 41 in page 39 show that as the distance between the crack tip and void increases, Mode II energy release rate with the void is approximately the same for the no void case. Fig. 42 in page 39 shows the ratio between the maximum values of Mode II energy release rate - obtained in Fig. 39 in page 38, Fig. 40 in page 38 and Fig. 41 in page 39 - for the void case and their corresponding value with no void. Fig. 42 in page 39 shows that the void have a great influence on Mode II when the void is close to the crack tip. Fig. 43 shows the angles at which Mode II is the maximum in Fig.39 in page 38, Fig. 40 in page 38 and Fig .41 in page 39. Also, Fig. 38 in page 37 shows that the maximum value of Mode II energy release is $100\,J/m^2$ at an angle of 30 degrees. Whether the crack will kink into the adhesive at this angle or no depends on the critical values for both Mode I and Mode II. Fig. 44, Fig. 45 and Fig. 46 show the total driving force obtained by the revised virtual crack closure technique (RVCCT) and the J-integral method. The behaviour shown in Fig. 38 in page 37 can be explained by examining the distribution of the stresses between the crack tip and the void. The dilatational energy density and the distortional energy denisty are used to give an indication about the stress distribution. The dilatational energy density is responsible for the volume exapnsion, while the distortion energy density is responsible for yielding.The equations for the dilatational and distortion energies are shown below:

$$Dilatational\ energy = U_V = \frac{1-2\nu}{6E}(\sigma_1+\sigma_2+\sigma_3)^2 \qquad (35)$$

$$Distortion\ energy = U_d = \frac{1+\nu}{6E}(\sigma_1-\sigma_2)^2+(\sigma_1-\sigma_3)^2+(\sigma_2-\sigma_3)^2 \qquad (36)$$

$$\nu = poisson\ Ratio$$

$$E = Young's\ Modulus$$

$$\sigma_1 = first\ Principal\ stress$$

$$\sigma_2 = second\ prinicpal\ stress$$

$$\sigma_3 = third\ principal\ stress$$

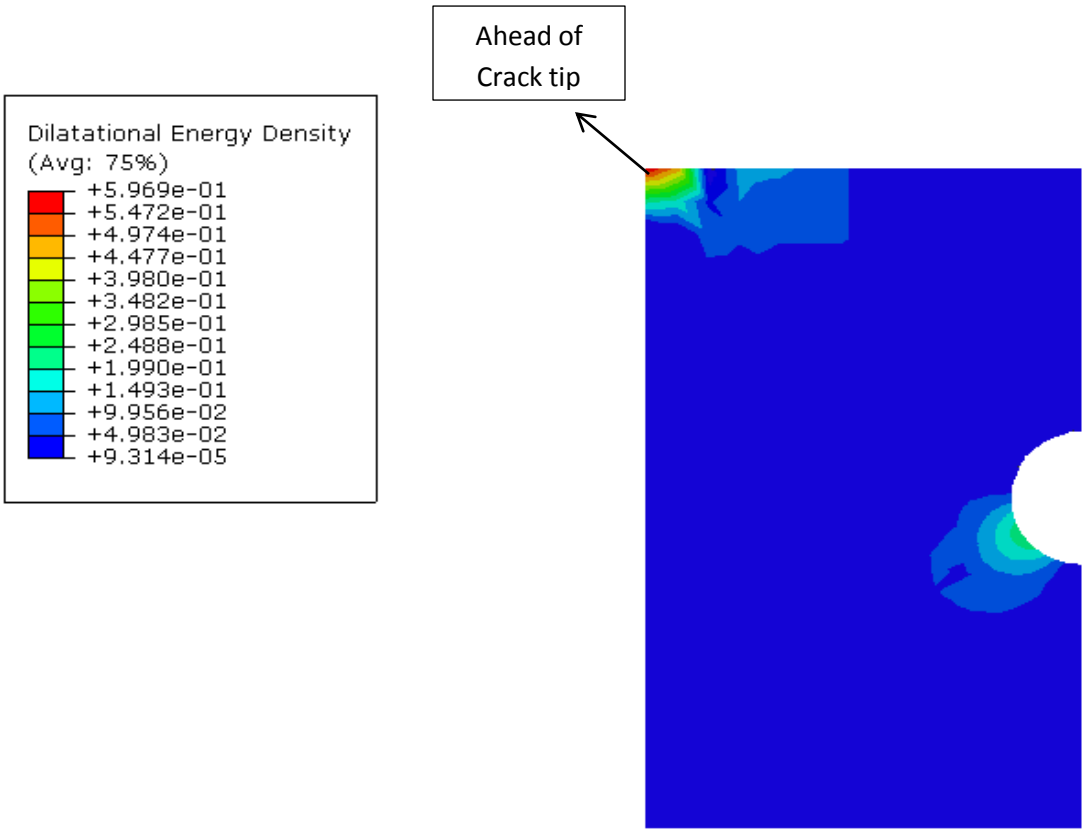

Fig. 47 Dilatational energy between void and crack tip.

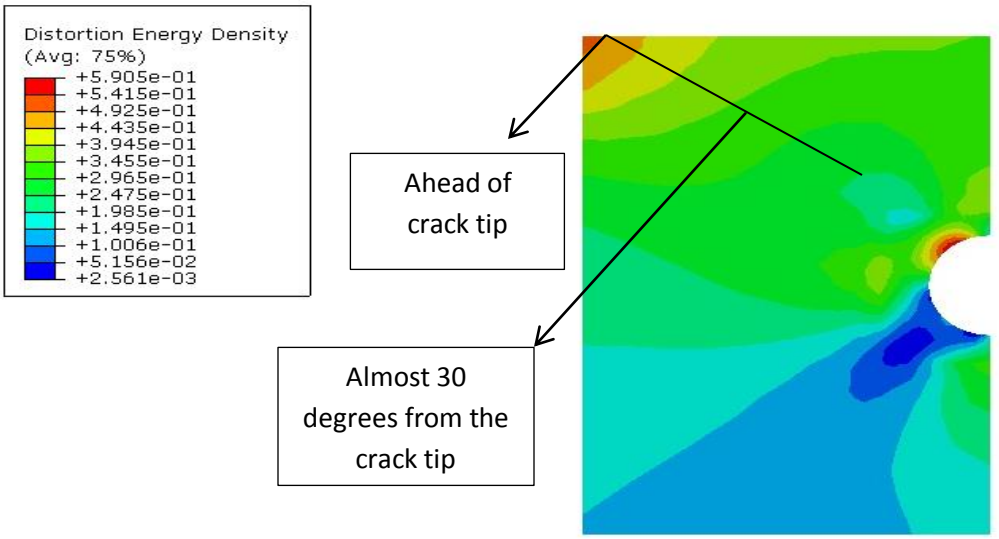

Fig. 48 Distortion energy between void and crack tip.

Fig. 47 and Fig. 48 show the dilatational energy density and distortion energy density respectiviely. Fig. 47 and Fig. 48 can be linked directly with the results shown in Fig. 36 in page 36 and Fig. 39 in page 38. Fig. 47 and Fig. 48 show that the dilatational energy density and distortion energy density are the highest near the crack tip, however the dilatational energy is a little bit higher than the distortion energy at the the crack tip and therefore, Mode I energy release rate at the interface is much higher than Mode II energy release rate. Also, Fig. 36 in page 36 show that it is highly difficult for a crack to propagate at another angle than zero in Mode I and that can be justified by the dilatiational Energy distribution in Fig. 47, where the dilatational energy density is the highest in the interface. Also From Fig. 39 in page 38, it is clear that the void can help the crack to kink from the interface into the adhesive and grow in Mode II - which is shear driven mode - at an angle of 30 degrees and this can be verified by examining the Distortion energy density in Fig. 48 , where the

distrotation energy is maximum at the interface and around the void at angle of 30 degrees from the interface as shown in Fig. 48.

III.D- Effect of the void radius on the energy release rate

From the previous study, it is evident that the critical void location is close to the crack tip, therefore the distance between the void and the crack - d1 - will be fixed to a distance of 0.3mm. Unfortunely there are very studies that reported the void radii within the adhesive film of a single lap joint, therefore the void radii used in this section will be adopted from [10]. These radii vary from 0.03mm-0.07mm with an increment of 0.02mm. Only one study conduted by Hadj-Ahmed [28] showed voids of radii approximately 0.03mm in the adhesive of a single lap joint.

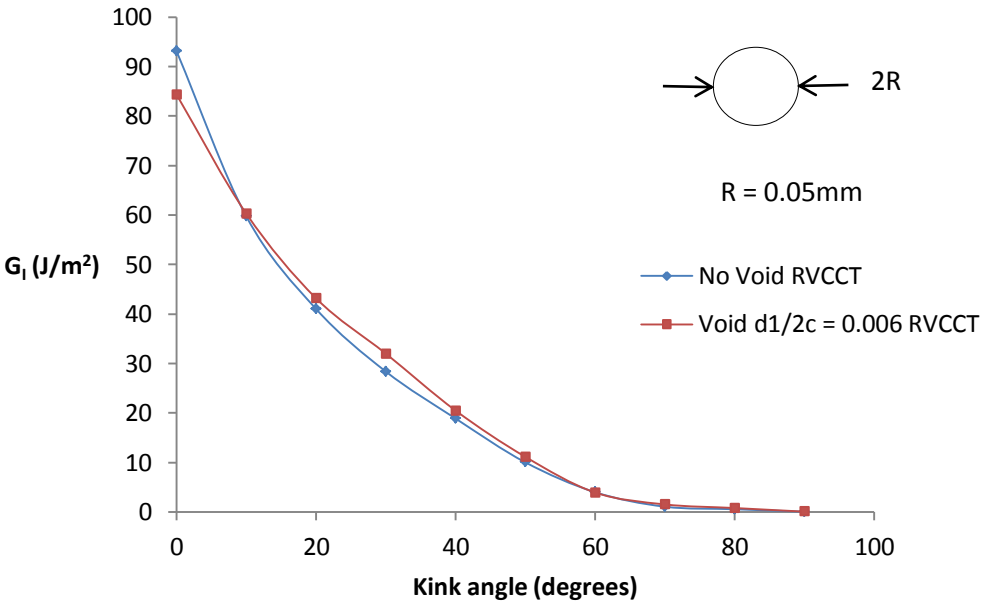

Fig. 49 Mode I energy release rate.

Mode I, Mode II and total energy release rates for a void with a radius of 0.03mm was studied in Fig. 36 in page 36 showed that the introduction of the void did not alter the Mode I energy release rate, however it had an impact on the Mode II energy release rate.

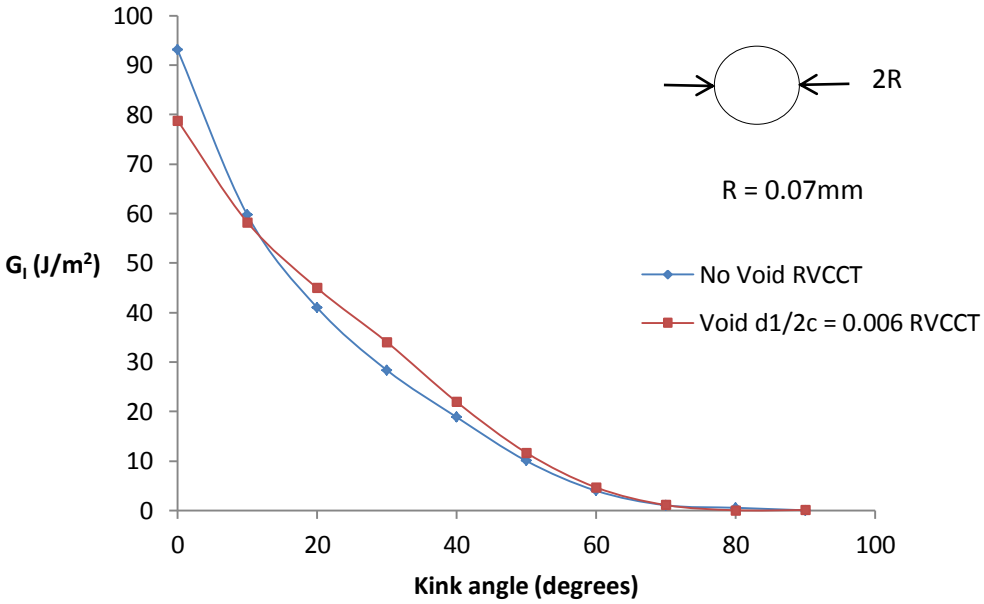

Fig. 50 Mode I energy release rate.

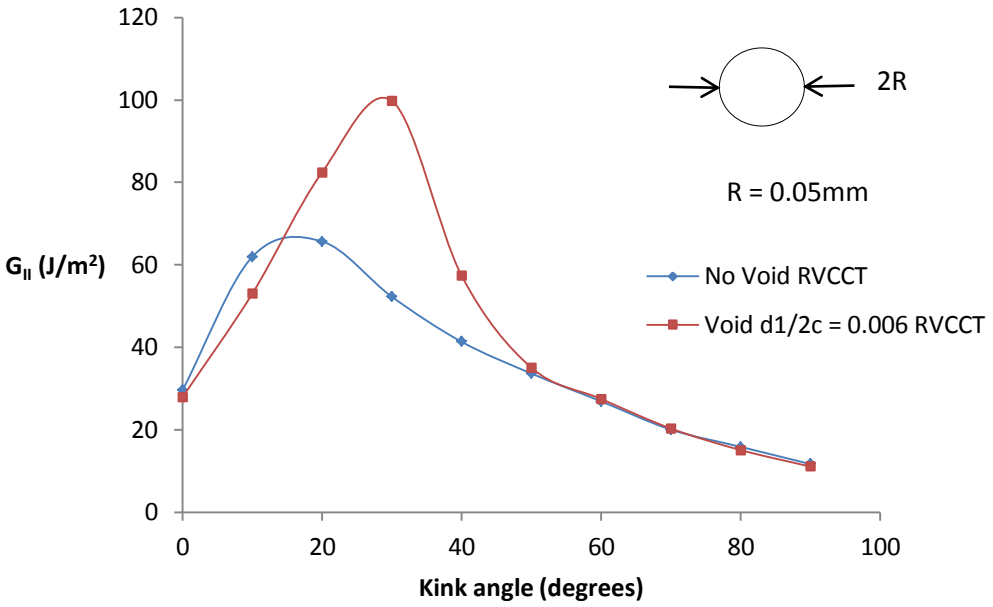

Fig. 51 Mode II energy release rate.

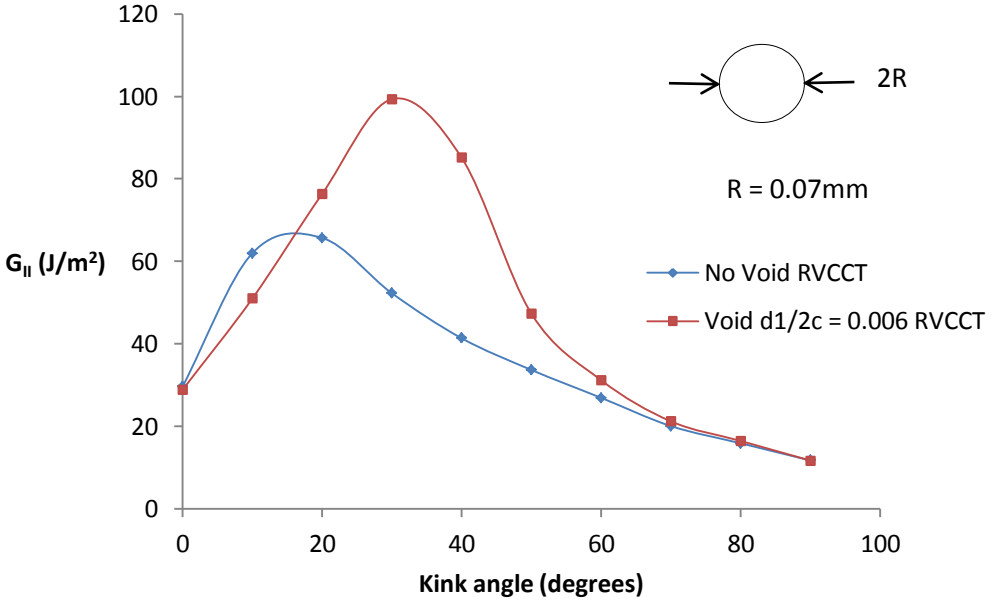

Fig. 52 Mode II energy release rate.

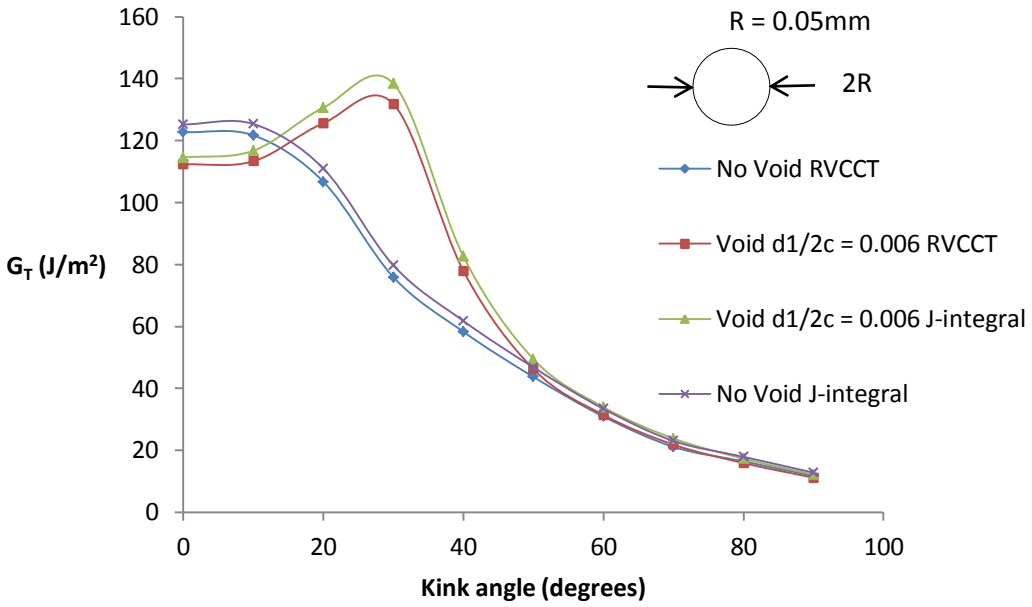

Fig. 53 Total energy release rate.

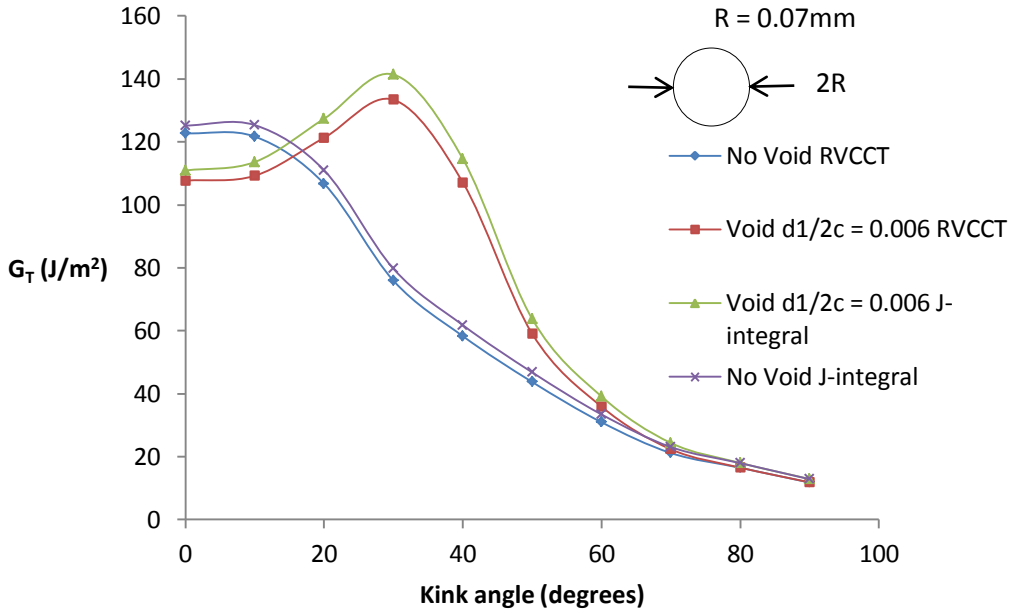

Fig. 54 Total energy release rate.

Fig. 49 in page 45, Fig. 50 in page 46, Fig. 51 , Fig. 52 , Fig. 53 , and Fig. 54 show that increasing the void radius did not have an effect on the pattern of Mode I, Mode II and the total energy release rates. For example, Fig. 49 in page 45 and Fig. 50 in page 46 show that as the void radius increases, Mode I energy release rate decreases at the interface. Also, Fig. 49 in page 45 and Fig. 50 in page 46 show that as the void radius increases, Mode I energy release rate increases over a range of 10 to 50 degrees, however these values are still less than value of Mode I energy release rate at the interface . Moreover, Fig. 51 and Fig. 52 show that increasing the void radius, increases Mode II energy release rate over a range of 30 to 50 degrees. Fig .50 in page 46 and Fig. 51 show that the highest value for Mode II energy release rate is at 30 degrees. Also, Fig .53 and Fig. 54 show the total energy release rate calculated by the revised virtual crack closure technique (RVCCT) and justified by the J-integral method for different void radii.

III.E- Effect of the void shape on the energy release rate

In this section the effect of the void shape on the energy release rate is examined.The void shape exaimed in this section is shown in Fig. 55. Different lengths - F - are examined to understand their effect on the energy release rate. Voids of such shape –Fig. 55- are expected to develop in the adhesive layer during the manufacturing of the single lap joint. The value of R is fixed to 0.03 mm and the distance from the crack tip - d1 - is fixed to 0.3 mm.

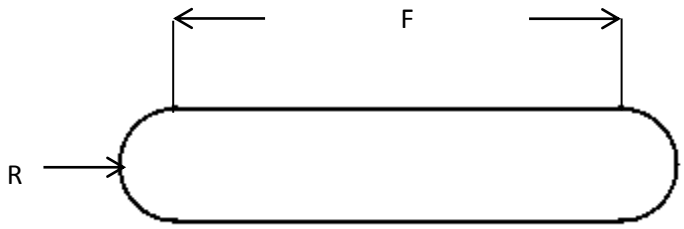

Fig. 55 Geometry of the studied void.

Also, when F is equal to zero the shape of the void is a circle with radius 0.03mm and this case was studied in the previous sections and the results are shown in Fig. 36 in page 36 and Fig. 39 in page 38.

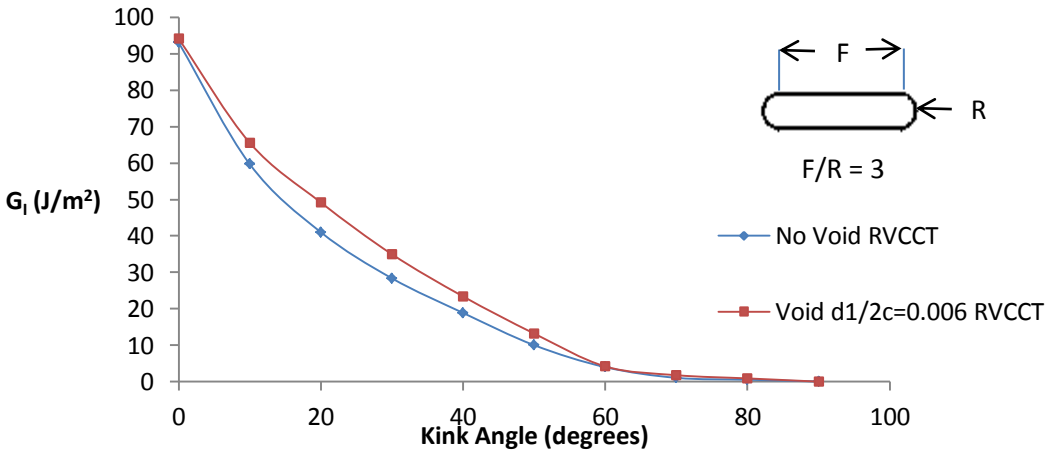

Fig. 56 Mode I energy release rate.

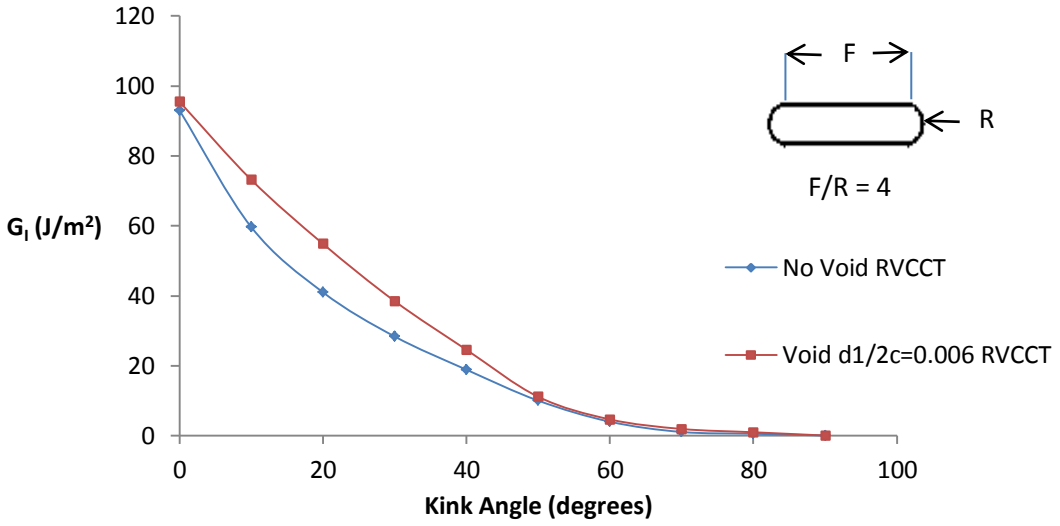

Fig. 57 Mode I energy release rate.

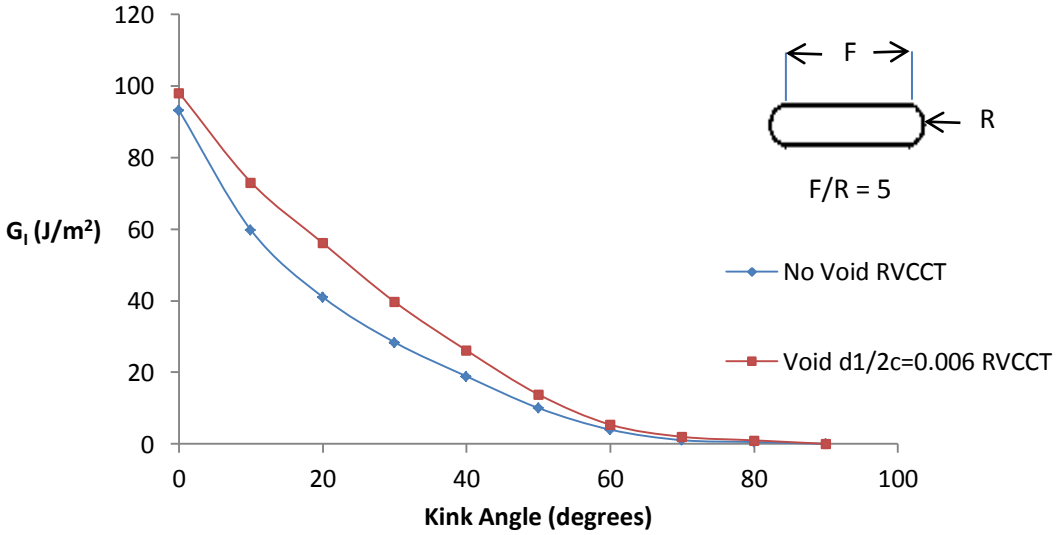

Fig. 58 Mode I energy release rate.

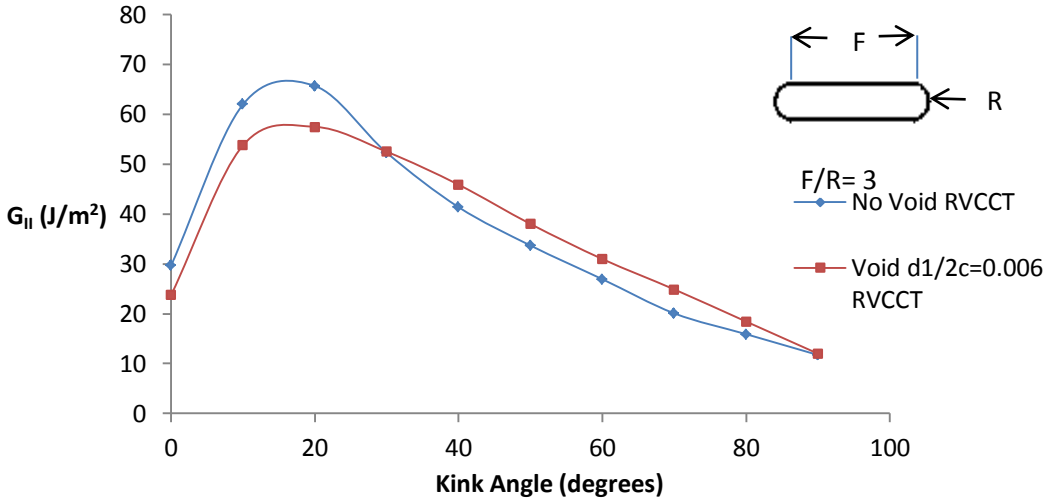

Fig. 59 Mode II energy release rate.

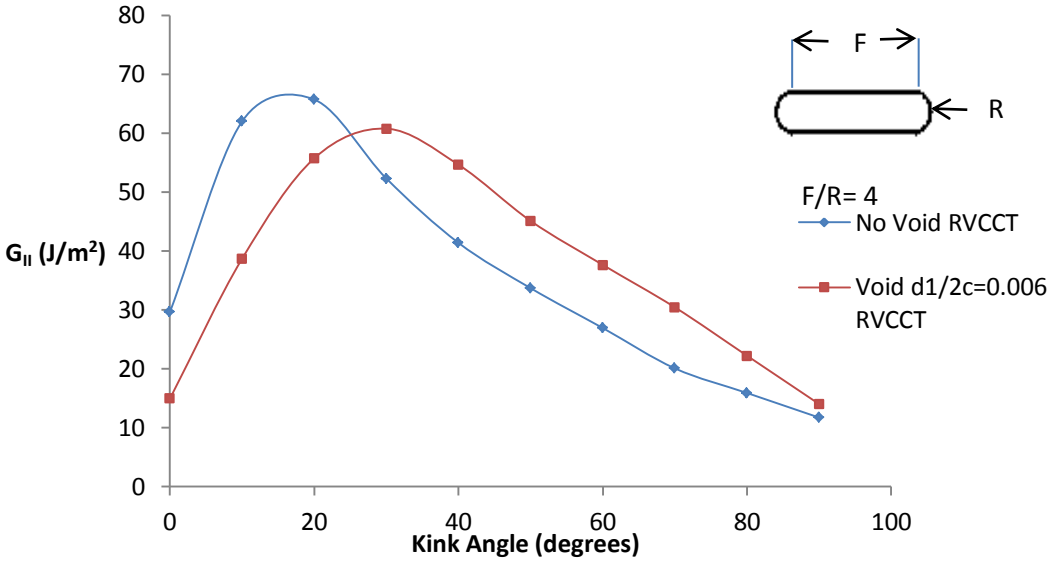

Fig. 60 Mode II energy release rate.

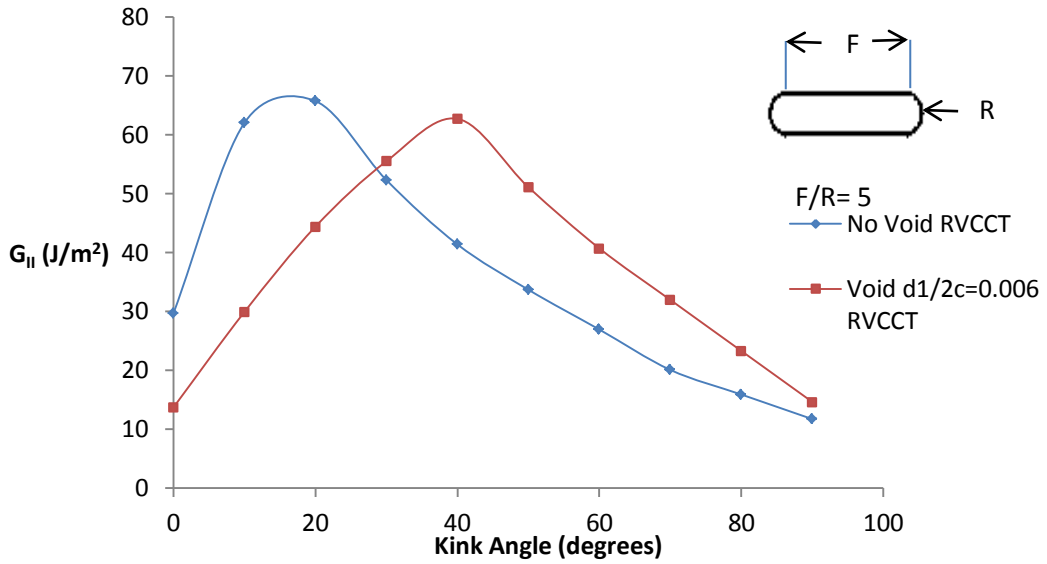

Fig. 61 Mode II energy release rate.

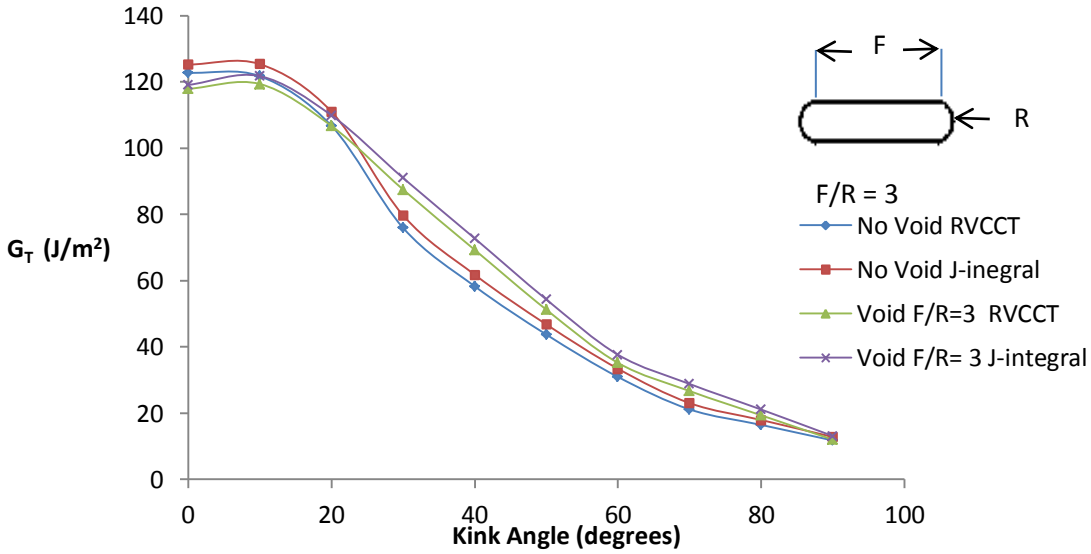

Fig. 62 Total energy release rate.

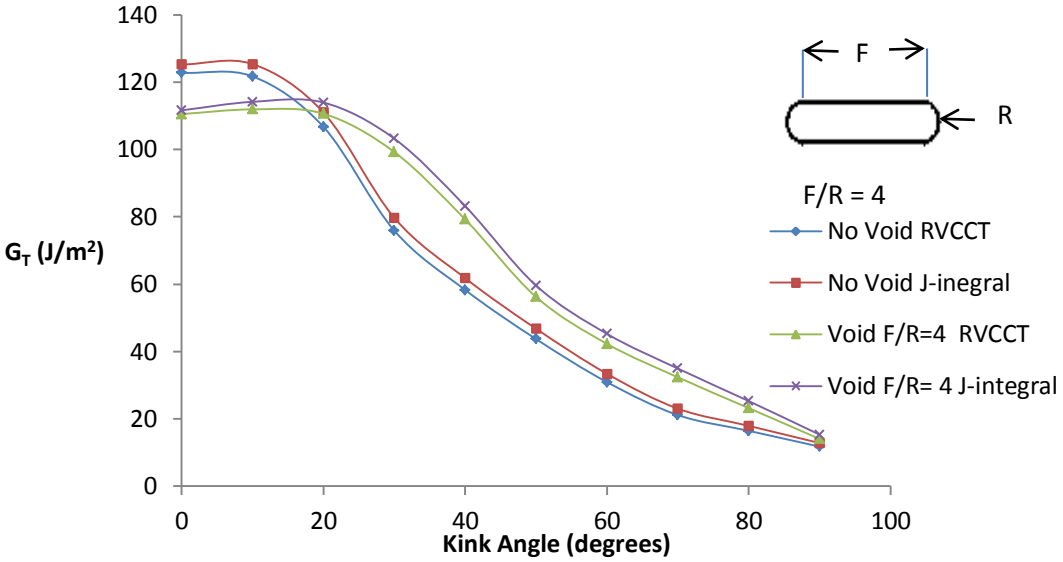

Fig. 63 Total energy release rate.

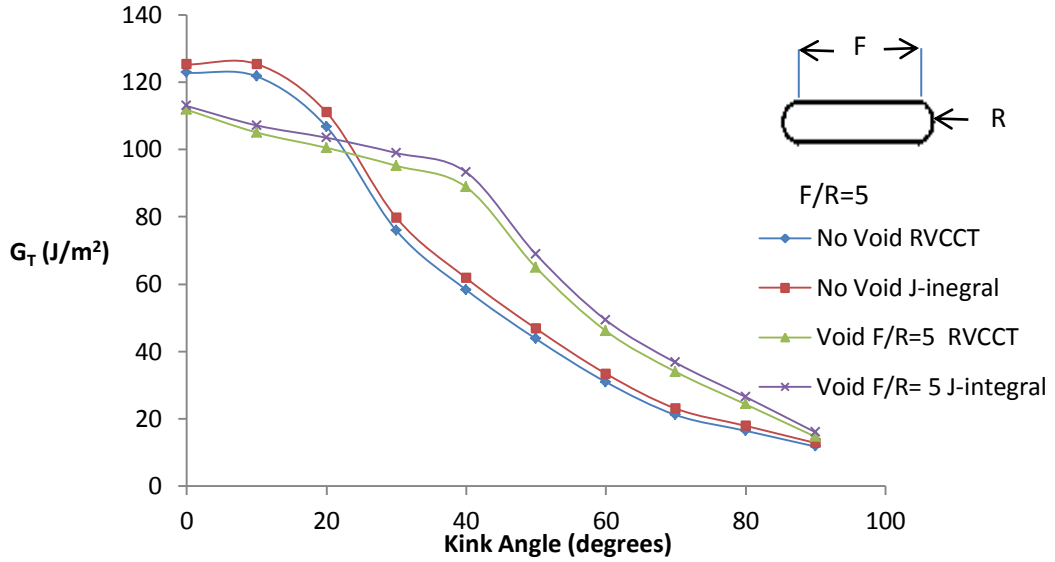

Fig. 64 Total energy release rate.

Fig. 53 in page 48, Fig. 54 in page 48 and Fig. 55 in page 50 show that as the ratio between the void length to the void radius increases, Mode I energy release rate at the interface

increases. Also, as the ratio between the void length to the void radius increases, Mode I energy release rate increases over 10 to 50 degrees range. Moreover, Fig. 59 in page 52, Fig. 60 in page 52 and Fig. 61 show that increasing the ratio between the void length to the void radius doesn't have an effect on the maximum value of Mode II energy release rate. Moreover, as the ratio between the void length to the void radius increases, the peak of Mode II energy release rate shift from the left to the right as shown in Fig. 59 in page 52, Fig. 60 in page 52 and Fig. 61. From Fig. 59 in page 52, Fig. 60 in page 52 and Fig. 61 Mode II energy release rate has a maximum value of 65 J/m^2 , which is less than Mode I energy release rate at the interface, therefore the crack will not kink into the adhesive. Finally, Fig. 61, Fig. 62 And Fig. 63 show the total energy release rate calculated by the revised virtual crack closure technique (RVCCT) and justified using the J- integral method. The distribution of the dilatational energy density and the distortion energy density between the crack tip and void can explain the behavior of Fig. 59 in page 52 and Fig. 61. The highest value of the dilatation energy and the distortion energy is ahead of the crack tip, however the value of the dilatational energy is larger than the value of the distortion enegy as shown in Fig. 65 and Fig. 66, therefore Mode I energy release rate is the higher than Mode II energy release rate at the interface. Fig. 66 shows the region where the distortion energy is high. This region is approximately 40 degrees from the crack tip, which explains why Mode II is high at 40 degrees in Fig.61. In addition, Fig. 47 in page 43 and Fig. 65 show that the dilatational energy for a circular void of radius 0.03mm - Fig.47 in page 43 - is lower than the dilatation energy for an elongated void - Fig. 65 - , which explains why the Mode I energy rate is lower at the interface for the circular void - Fig. 36 in page 36 - when compared with an elongated void - Fig. 58 in page 51 -.

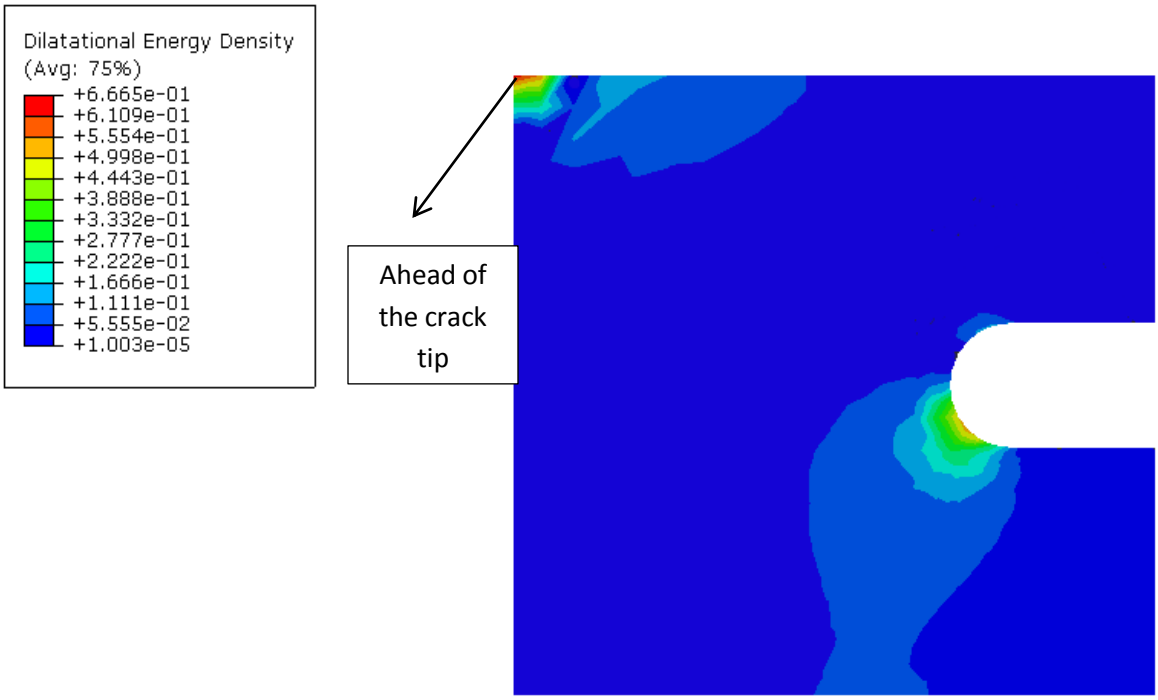

Fig. 65 Dilatational energy density.

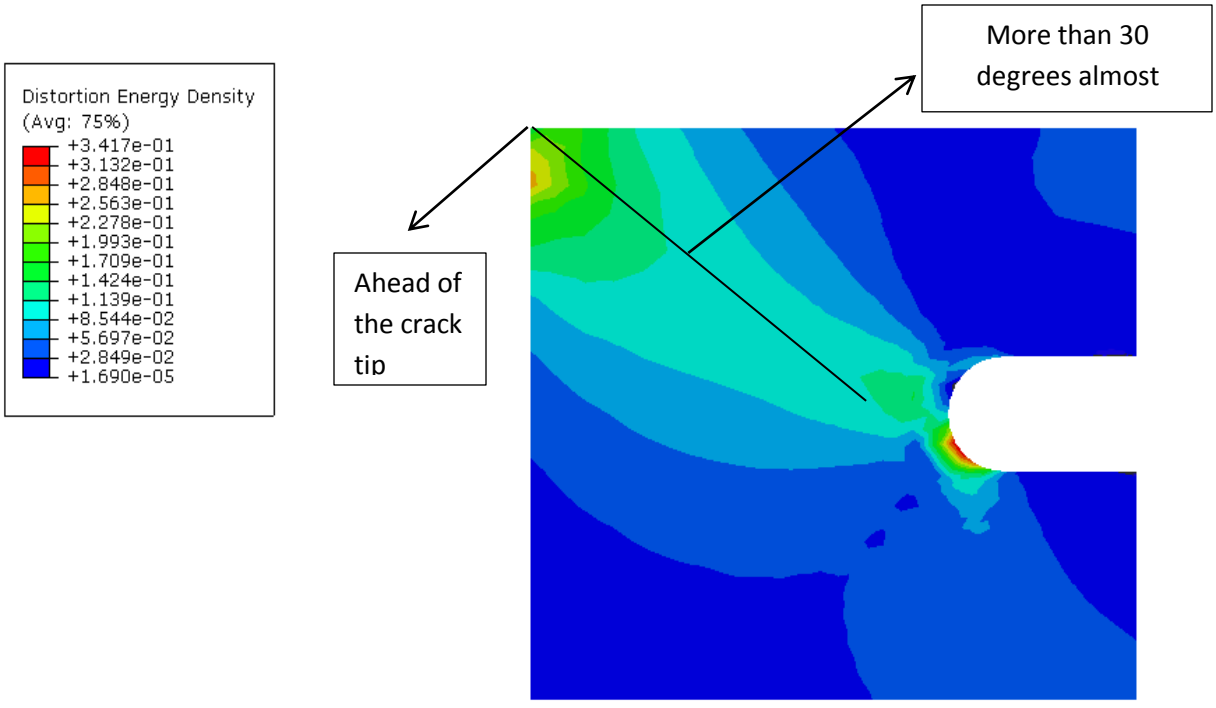

Fig. 66 Distrotion energy density.

Also, the distortion energy of a ciruclar void of radius 0.03mm – Fig. 48 in page 44 – is higher than distortion energy of an elongated void – Fig. 66 – which explains why Mode II of a circular void 0.03mm – Fig. 39 in page 39 – is higher than Mode II of an elongated void – Fig. 61 in page 53–.

III.F- Effect of multiple cracks without void on the energy release rate

In this section, the effect of two cracks without a void in the adhesive is examined. As discussed previously in Fig. 4 in page 3, the maximum stresses occur at the end points in the interface between the adhesive and adherends - points C&D -. Previously a crack was embeded in the upper left interface between the adhesive and adherend. Another extra crack is embedded in the lower right interface between the adhesive and the adherend where the stresses are the maximum. The distance between the two crack is very small – 1mm – to see how they interact. One crack will is assumed to grow a small distance of 0.1mm at different angles, as shown in Fig. 35 in page 36, while the other is held stationary and vice versa.

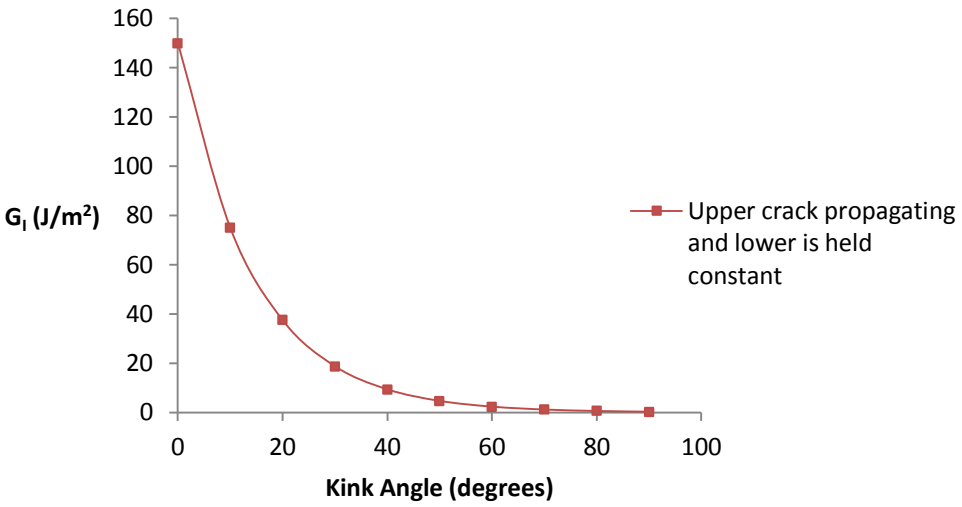

Fig. 67 Mode I energy release rate.

Fig. 67, Fig. 68 And Fig. 69 Show Mode I, Mode II and the total energy release rate for different paths of the upper crack, while the lower is held stationary. Fig. 67 and Fig. 68 show that Mode II energy release rate is very high when compared with Mode I energy release rate.

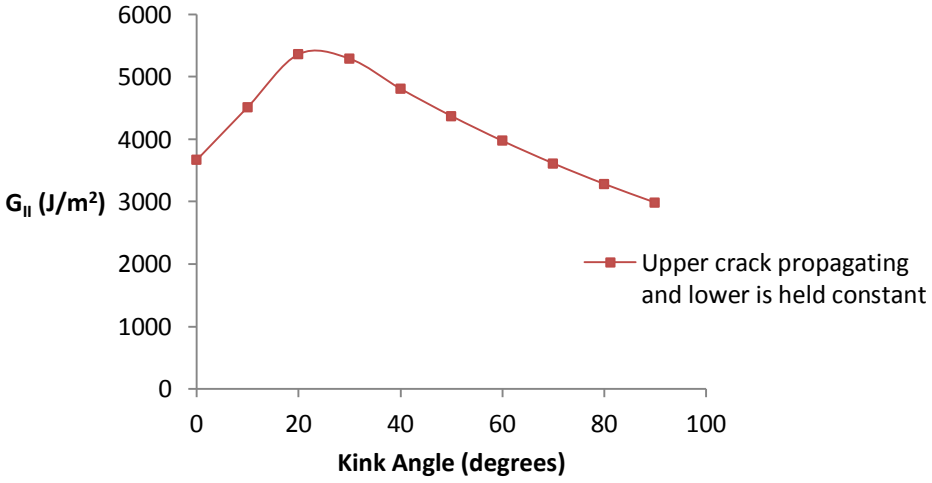

Fig. 68 Mode II energy release rate.

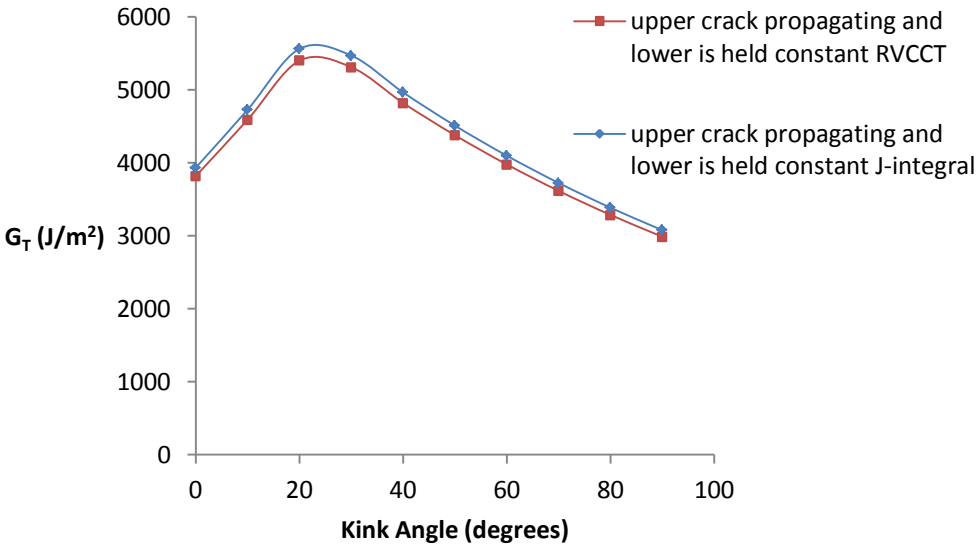

Fig. 69 Total energy release rate.

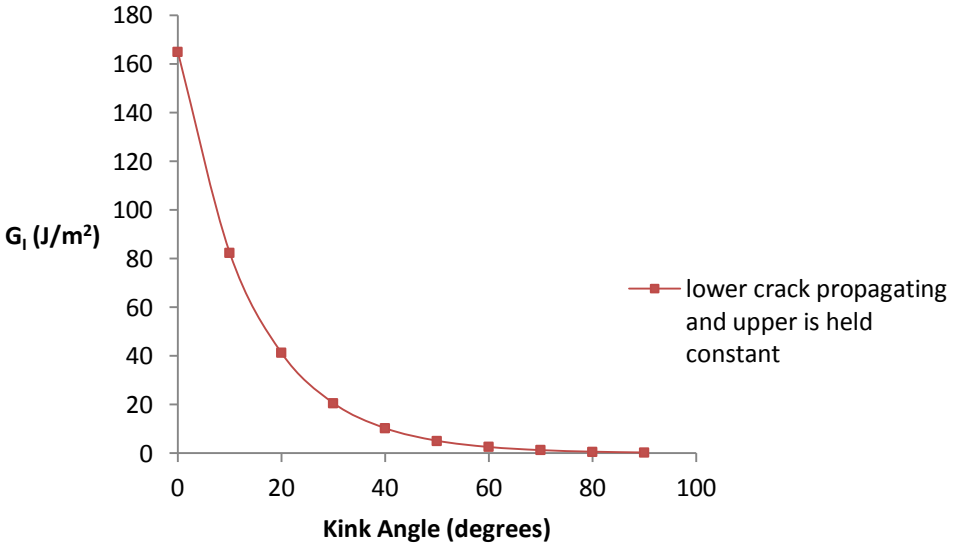

Fig. 70 Mode I energy Release rate.

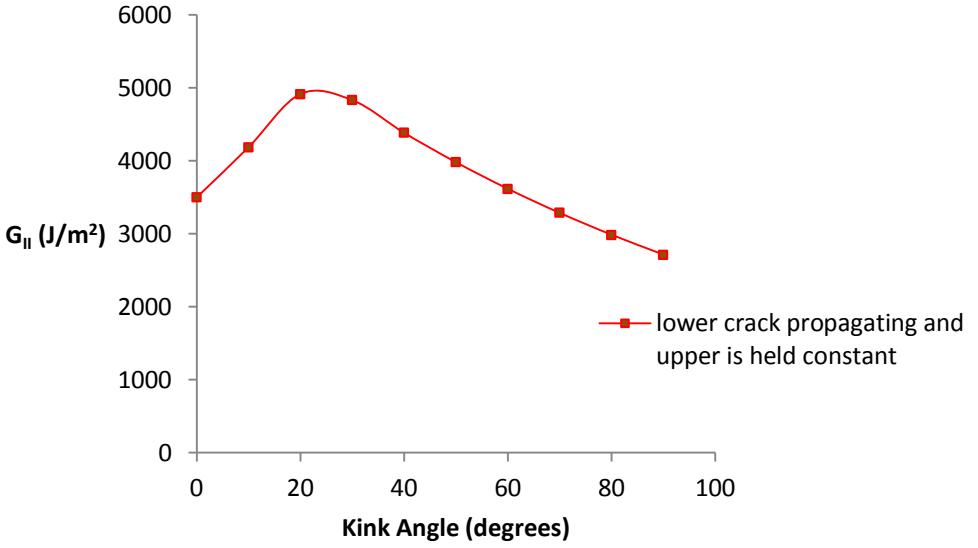

Fig. 71 Mode II energy release rate.

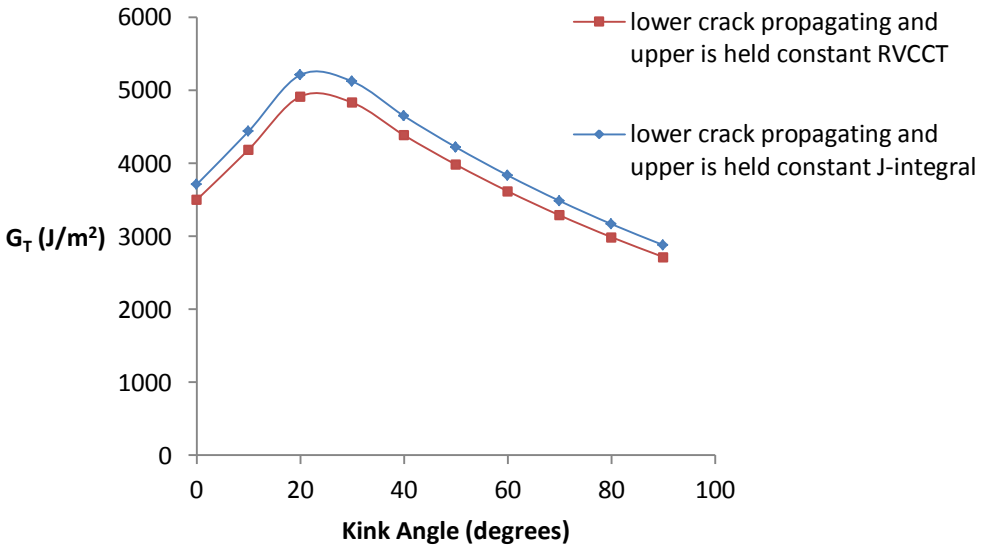

Fig. 72 Total energy release rate.

Fig. 67 and Fig. 68 show that Mode I has a maximum value of approximately 150 J/m^2 at the interafce and Mode II has a maximum value of approixmately 5500 J/m^2 at an angle that

ranges from 20 to 30 degrees. Mode II has a very high value compared to Mode I, which means that the crack might grow in Mode II from the interface at an anlge of 20 degrees. This high Mode II energy release rate might be attributed to the presence of another crack at the lower interface, which means that the two cracks are interacting with each others. Also, Fig. 69 shows the total energy release rate caluculate by the revised virtual crack closure technique (RVCCT) and justified by the J-integral Method. The lower crack shows a similar behaviour in the energy release rates of Mode I and Mode II as shown in Fig. 70, Fig. 71 And Fig. 72 . The dilatational energy density and the distortion energy density of the region between the two crack is examined to undestand the results shown from Fig. 67 in page 58 to Fig. 72.

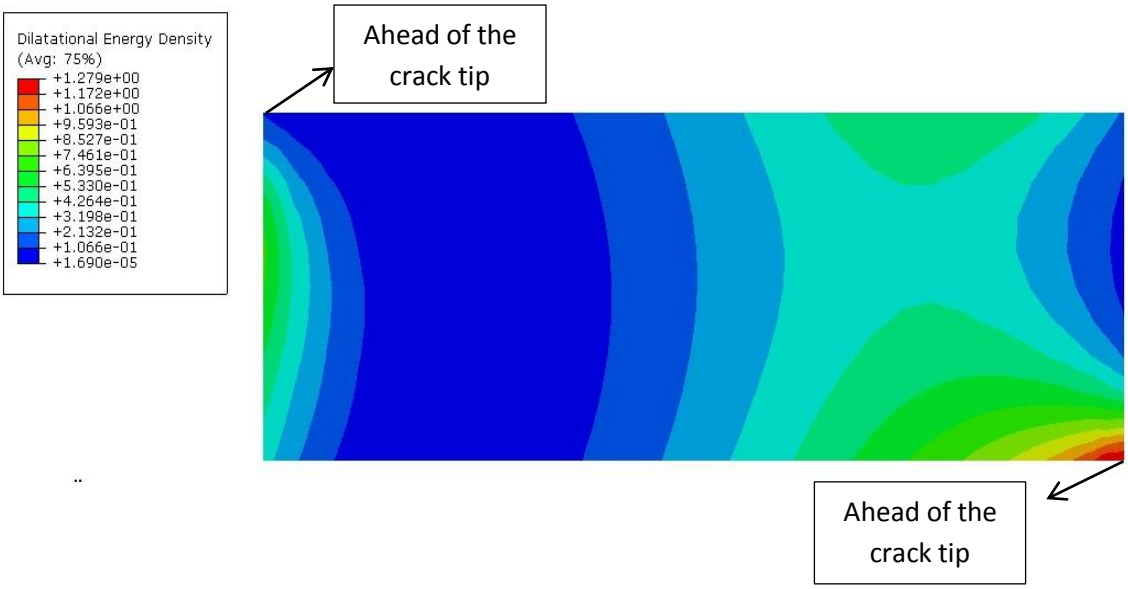

Fig. 73 Dilatation energy density between the two cracks.

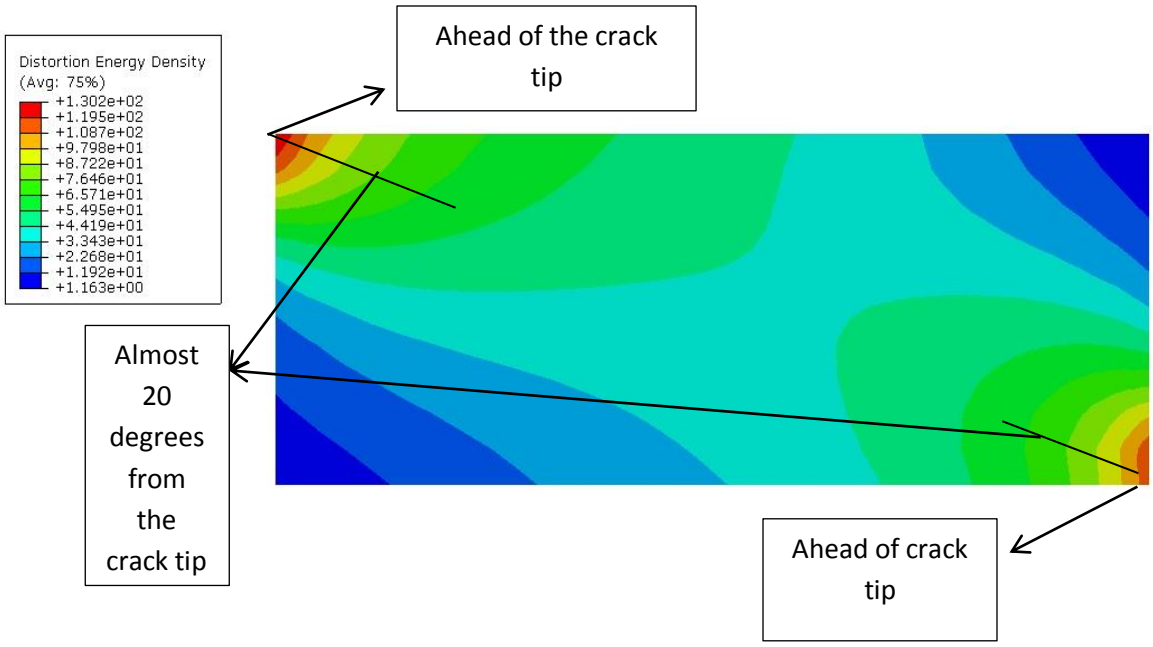

Fig. 74 Distortion energy density between the two cracks.

Fig. 73 and Fig. 74 show the dilatational and distortion energy respectiveley. The distrotion energy is much higher than the dilatational energy , which explains why Mode II is much higher than Mode I. Also, It is clear from Fig. 74 that the two cracks are interacting with each other, as if they are pulling one another and that is the reason why Mode II is the highest at angle of 20 from both cracks, which is approximately the shortest distance between the two cracks.

III.G- Effect of a biased void and multiple cracks on the energy release rate

In the previous section, the effect of two cracks without the effect a void was examined. In this section, a void that is closer to the upper crack than the lower crack is introduced. The void is placed at a distance of 0.3mm from the upper crack tip.

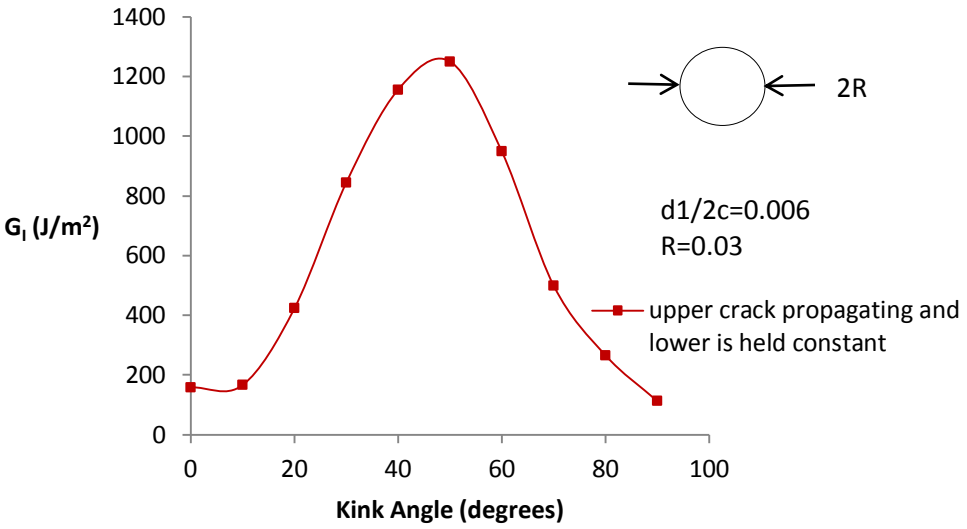

Fig. 75 Mode I energy release rate.

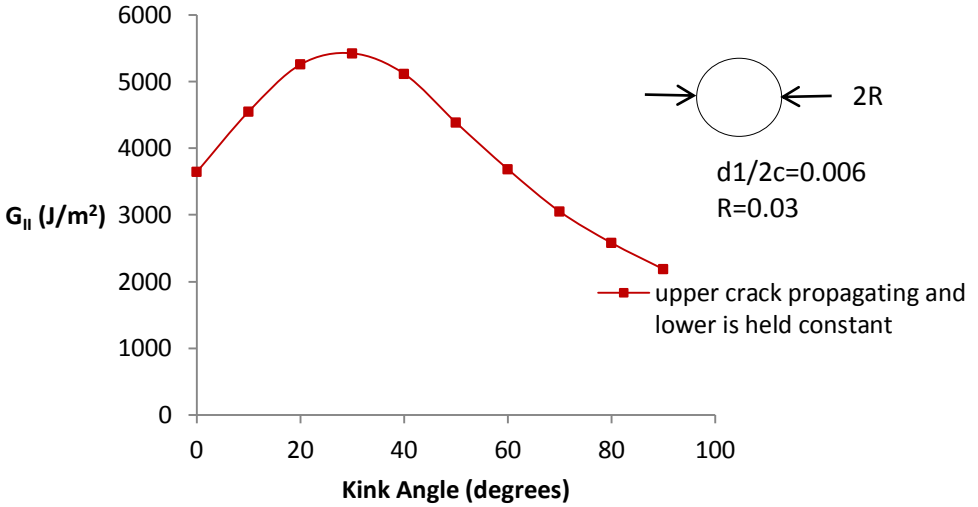

Fig. 76 Mode II energy release rate.

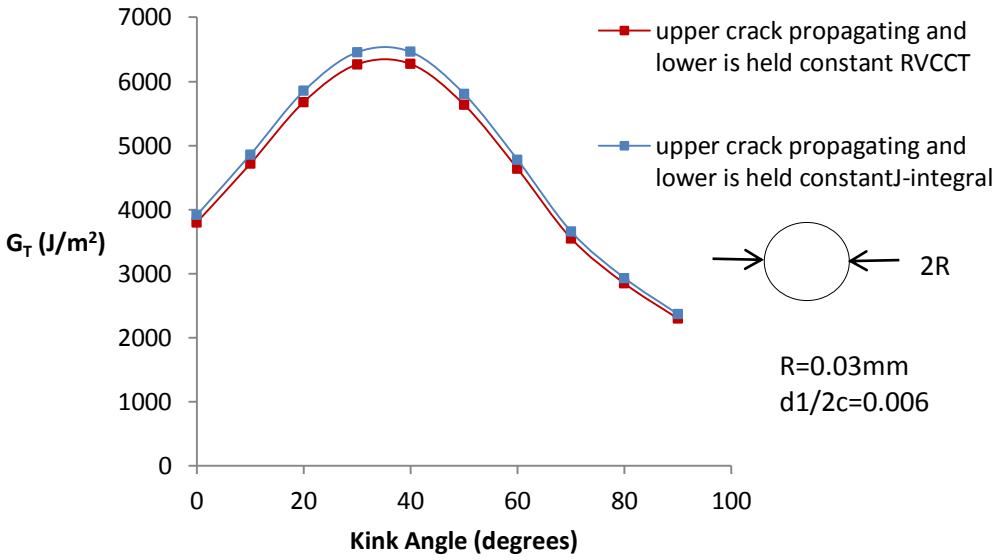

Fig. 77 Total energy release rate.

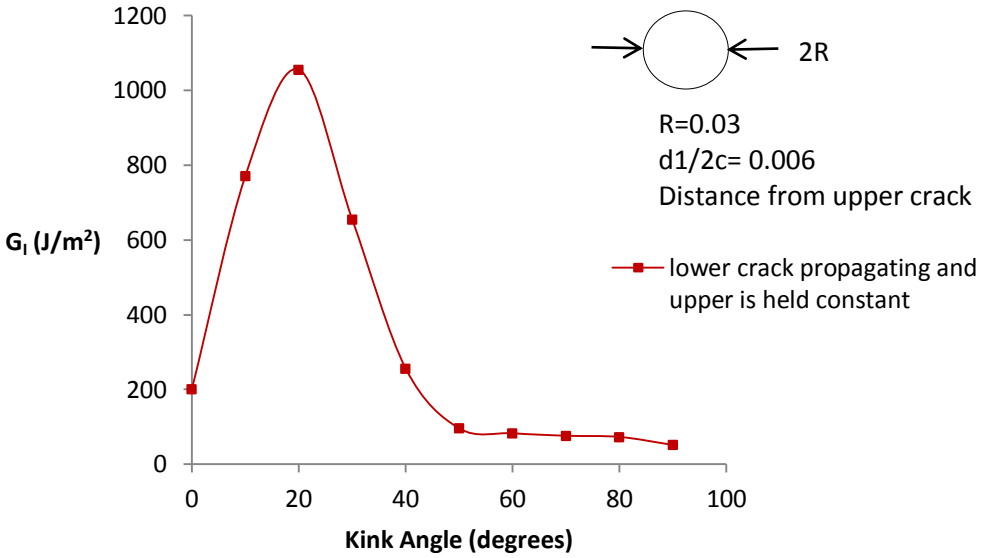

Fig. 78 Mode I energy release rate.

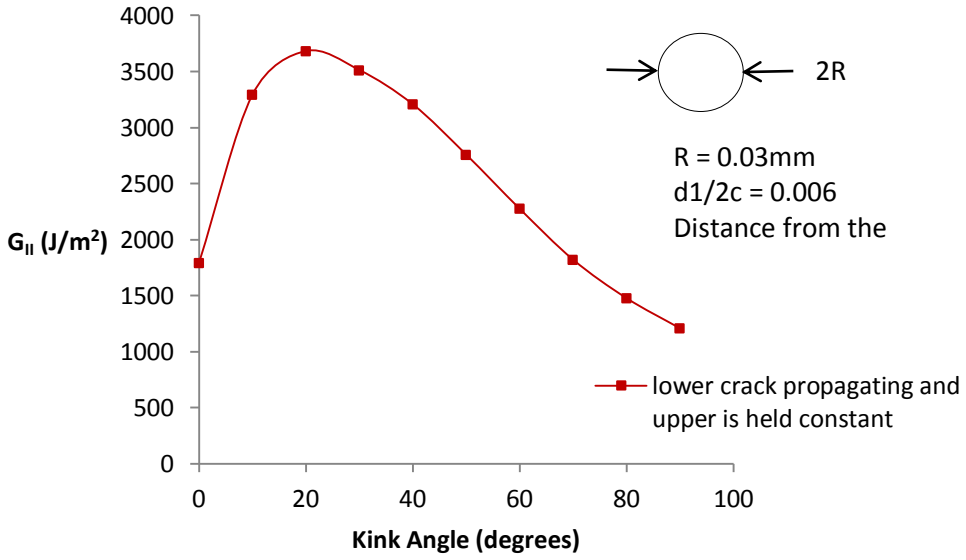

Fig. 79 Mode II energy release rate.

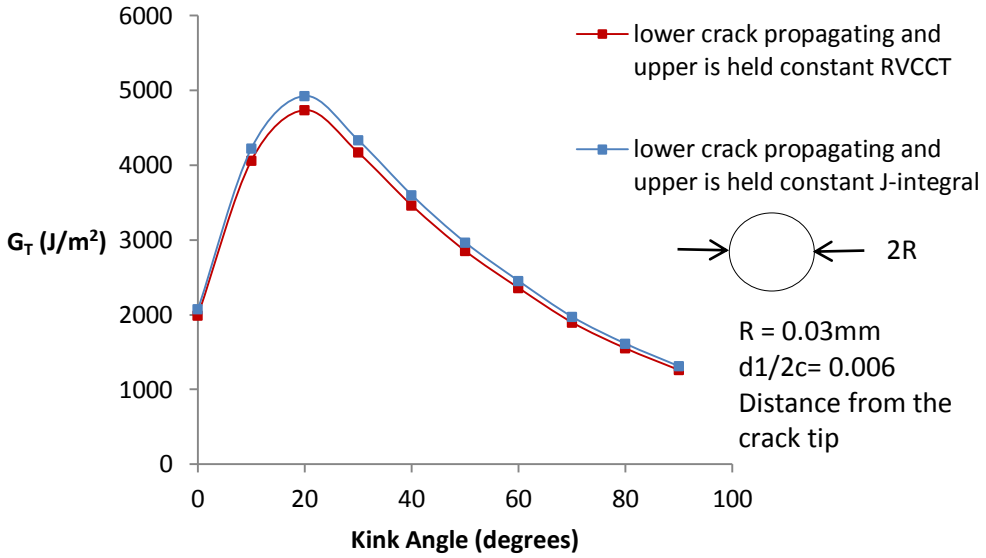

Fig. 80 Total energy release rate.

Fig. 75 in page 63 and Fig. 78 show that the introducation of a void between the two cracks affected the pattern of Mode I energy release rate when compared with the non void case – Fig. 67 in page 58 and Fig. 70 in page 59 – Moreover, Fig. 76 and Fig. 79 show that the introduction of a void between the two cracks did not have an effect on the pattern of Mode II energy release rate. Also Fig. 77 and Fig. 78 show the total energy release rates calucated by the revised virtual crack closure technique (RVCCT) and justified by the J-integral Method. From Fig. 75 in page 63, the maximum value of Mode I energy release rate is 1200 J/m^2 at an angle of 40 degrees. Also, From Fig. 78 the maximum value of Mode I is 1000 J/m^2 at an angle of 20 degrees. Fig. 76 Shows a maximum of 5500 J/m^2 for Mode II energy release rate at an angle of 30 degrees. Mode I and Mode II for the lower and the upper cracks have different values at diffferent angles due to the fact that the void is closer to the upper crack than the lower crack. The dilatational energy and the distortional energy distribution between the two cracks is examined and their results can be linked directly to

Fig. 75 in page 63, Fig. 76 in page 64, Fig. 77 in page 64 and Fig. 78 in page 65. Fig. 81 shows that the introduction of a void in the adhesive film between the two cracks raised the dilatational energy density when compared with non void case. Also, Fig. 81 shows that the dilatational energy density is the maximum around void. The behaviour shown in Fig. 75 in page 63, where Mode I energy release rate increases from 10 degrees to 40 degrees can be explained by Fig. 81, where the dilatational energy density is the maximum in the range of these angles. The behaviour of Mode II shown in Fig. 77 in page 64 and Fig. 78 in page 65 can be linked to the distortion energy density - Fig. 82-. Fig. 76 in page 64 and Fig. 78 in page 65 show a maximum of Mode II at angles of 20 and 30 degrees respecitevley and this can be explained by looking at the maximum locations of the distortion energy density - Fig. 82 -, where the maximum is ahead of the two cracks and at certain locations around the void which almost conicide with these angles.

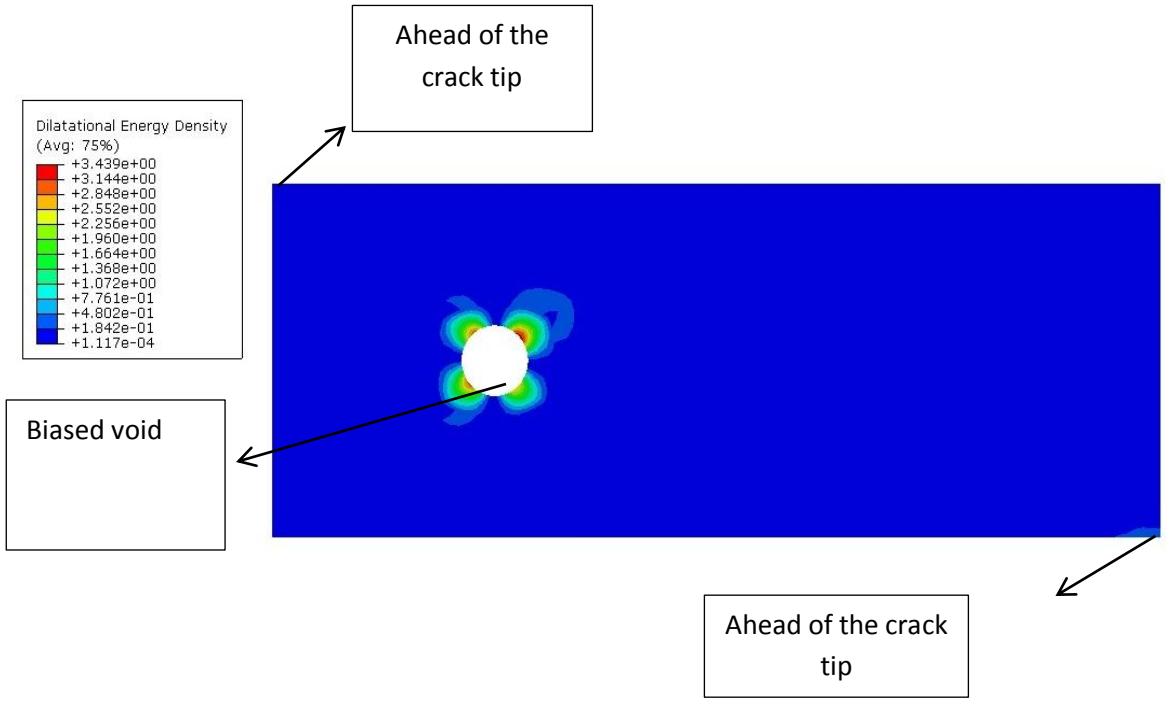

Fig. 81 Dilatation energy density with a void between two cracks.

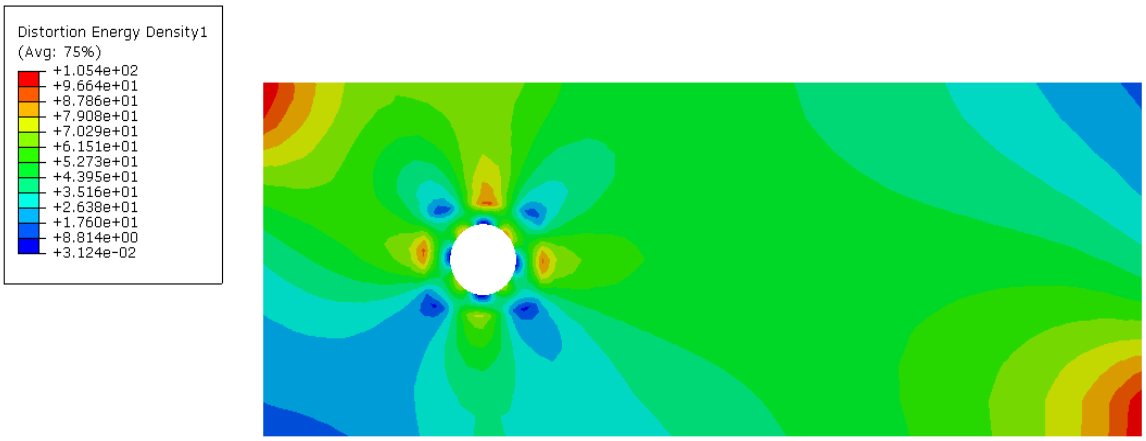

Fig. 82 Distortion energy density with a void between two cracks.

III.H- Effect of two voids and two cracks on the energy release rate

In the previous section, the effect of one biased void and two multiple cracks was examined. In this section two voids and two multiple crack will be studied. One void is placed at a distance of 0.3mm from the upper crack tip, while the other void is placed at 0.3mm from the lower crack tip in middle of the adhesive. The energy release rate for each crack will be computed separately.

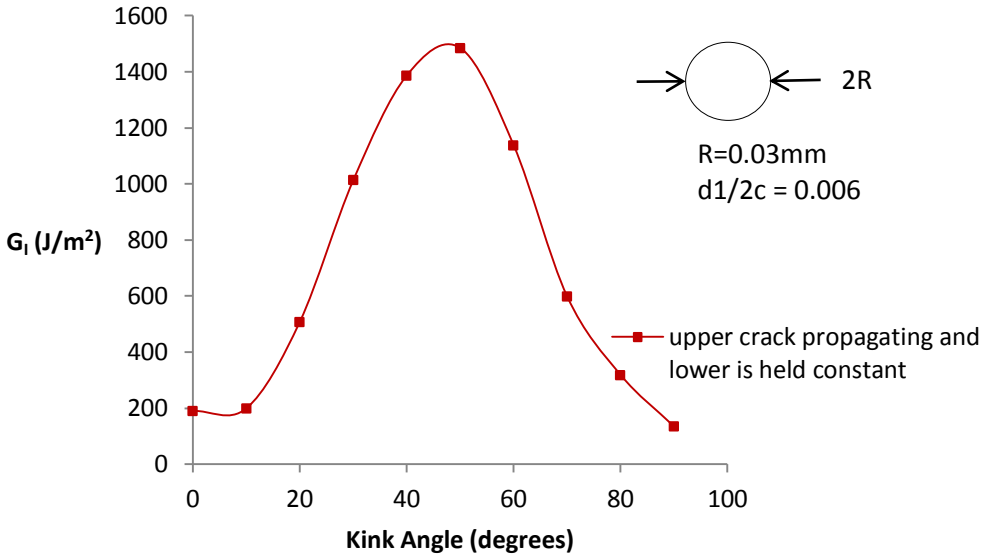

Fig. 83 Mode I energy release rate.

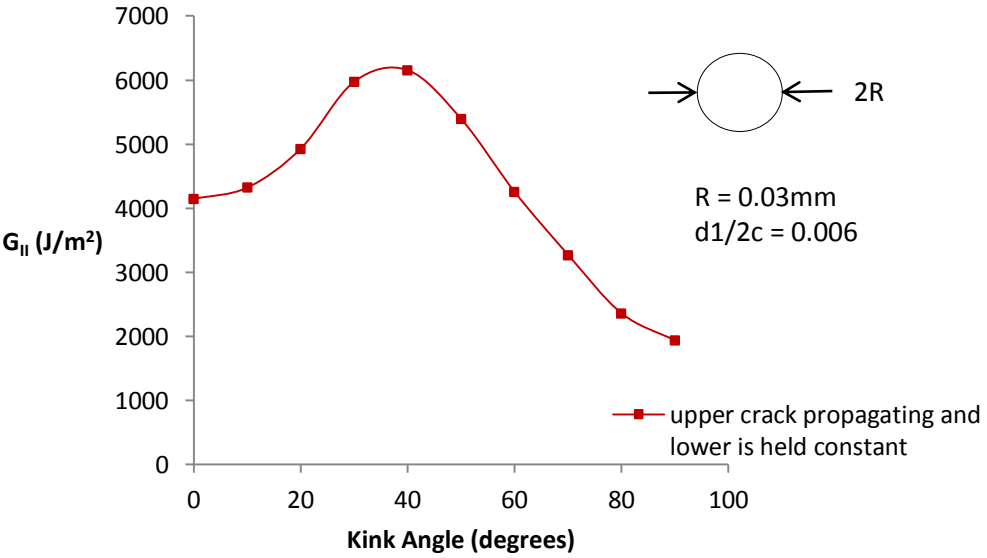

Fig. 84 Mode II energy release rate.

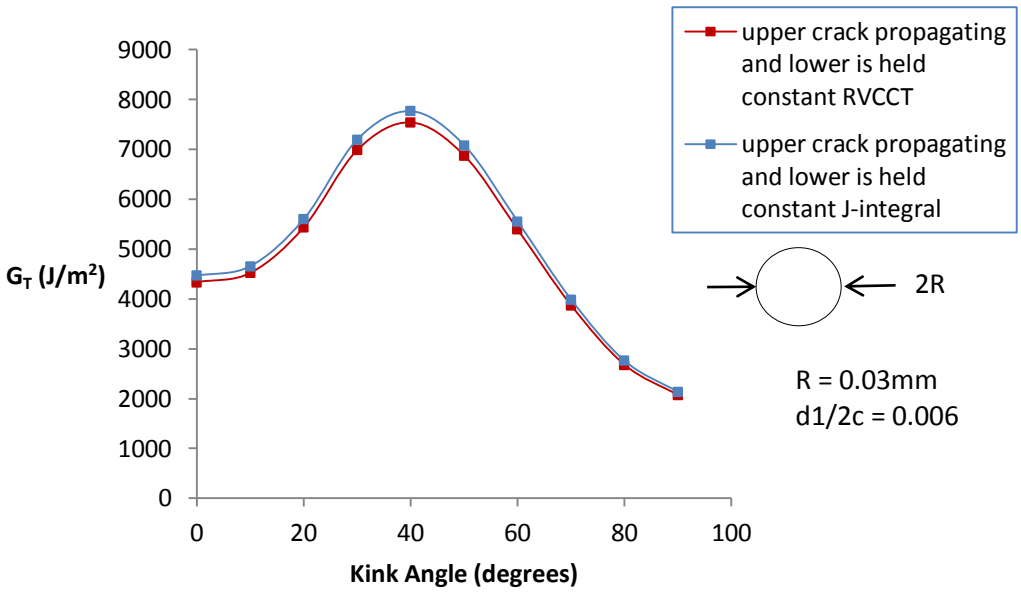

Fig. 85 Total energy relase rate.

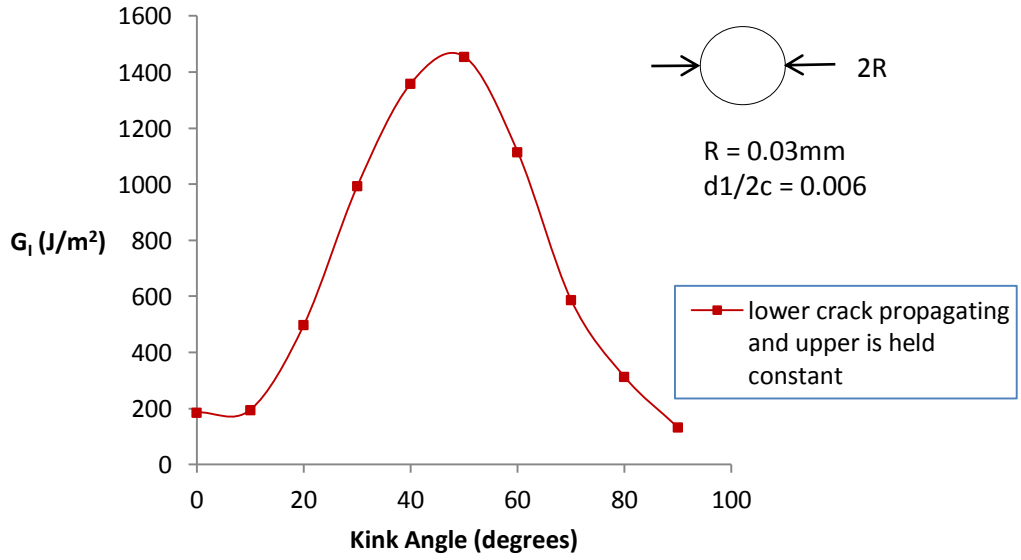

Fig. 86 Mode I energy release rate.

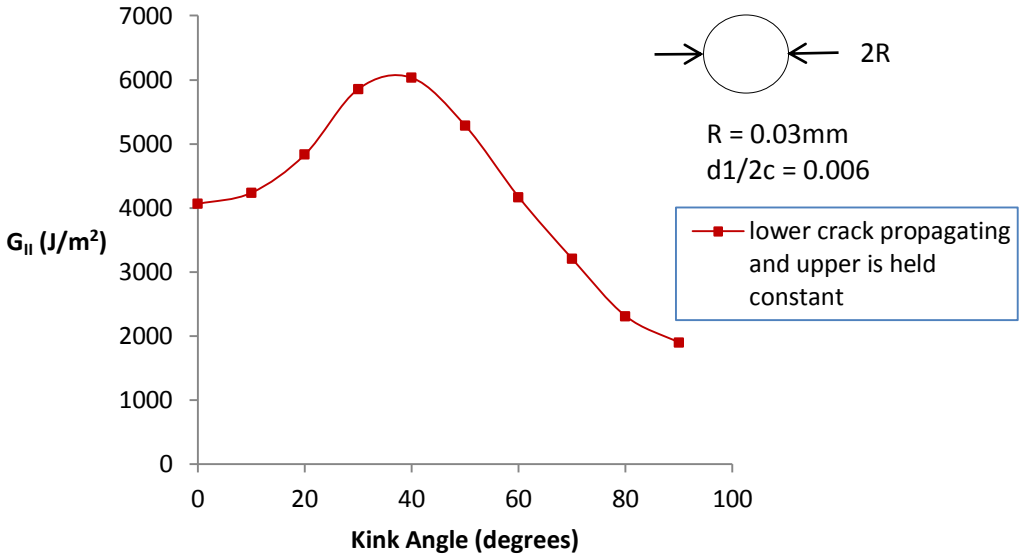

Fig. 87 Mode II energy release rate.

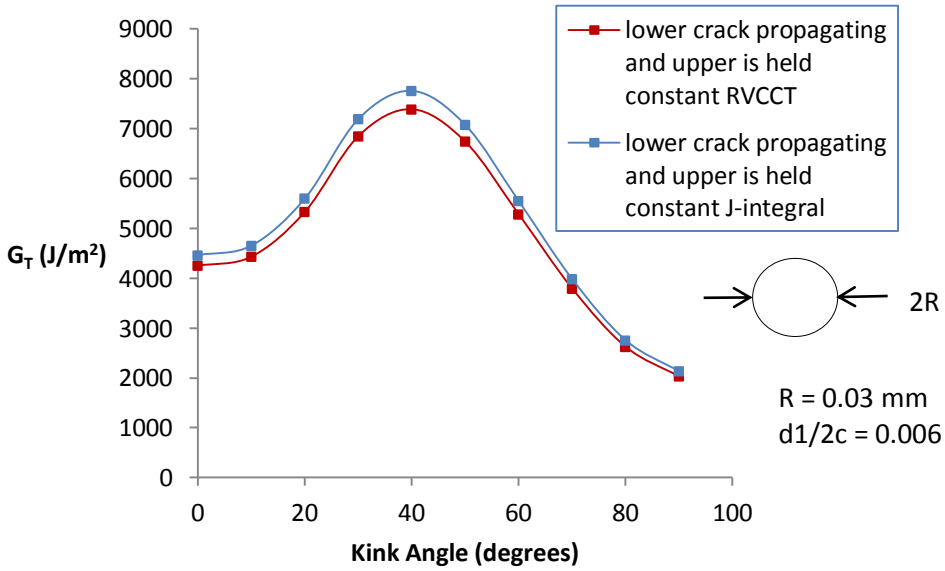

Fig. 88 Total energy relase rate.

Fig. 83 to Fig. 88 show that the introduction of another void increased Mode I, Mode II and the total energy release rate. The value and pattern of energy release rates for the upper crack

and the lower crack are almost similar and that is due to the symmetry of the problem, as the two voids are placed at the same distance from the upper and the lower crack. Finally, Fig. 85 and Fig. 88 show the total energy release rate calculate by virtual crack closure technique (RVCCT) and justified by the J- integral method. Also, from Fig. 89 and Fig. 90 the introducation of a new void increased both the Dilatational and distortion energy.

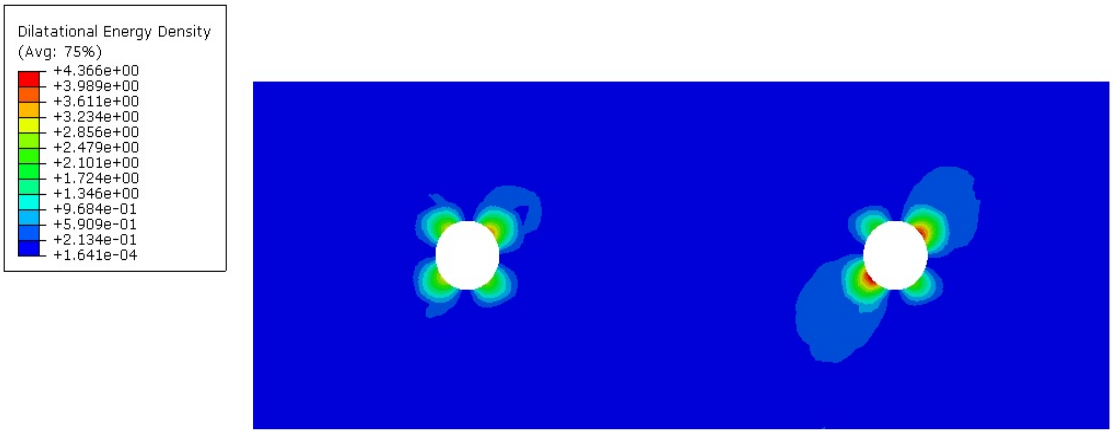

Fig. 89 Dilatational energy density of two voids between two cracks.

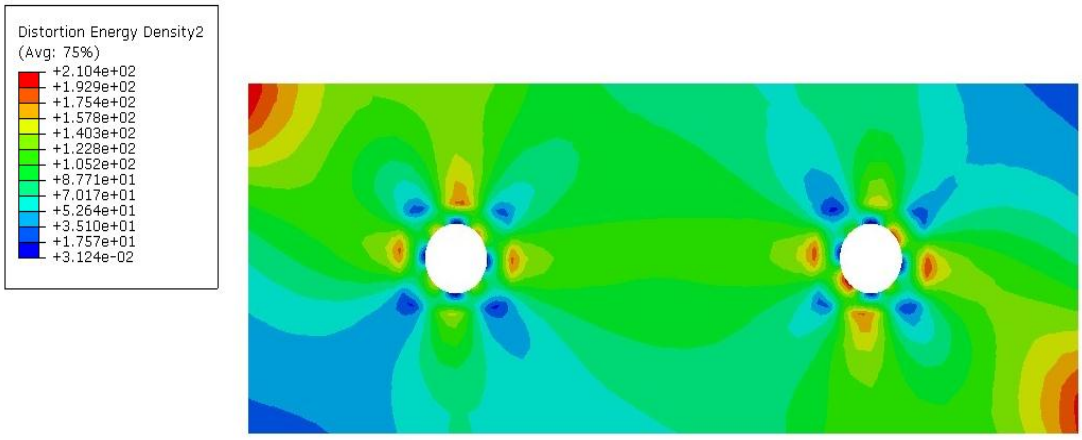

Fig. 90 Distortion Energy density of two voids between two cracks.

CHAPTER IV

CONCLUSION

The main objective of this study is to understand how a void might help an interface crack in a single lap joint to kink into the adhesive film based on the energy release rate method. Consideration is given to several factors such as void radius, void distance, void shape, multiple voids and multiple cracks. By studying the effect of these factor, the effect of a void on the crack kinking process could be understood. By using NDT the size of the void, the shape of the void and the location of a void could be easily detected in the adhesive film of a cracked single lap joint. The information obtained from NDT would help the engineers and manufacturers in the durability assesment of the sinlge lap joints by determining the critical size, location and shape of the void.

From the studies conducted in the previous sections, It is obvious that the most prominent factor is the location of the void from the crack tip. The Closer the void to the crack tip, the larger the effect on the energy release rate.

Voids play an important role in the failure of any component. Unfortunetly there are very few studies on how voids could lead to failure of a single lap joint, therefore it is essesntial to conduct some experiments to understand how voids could lead to the final failure. These experiments would help in understanding the effect of void parameters on the failure mechanism. Although these experiments are essential , however they are very hard, expensive and time consuming, therefore the best way to understand the effect of these parameters is through numerical studies, which is faster and cheaper.

Finally, for Future work, the effect of other parameters such as: the fiber orientation in the adherends, the thickness of the adherends, the thickness of the adhesive and the length of the adhesive will be taken into consideration. Also, the complete crack path will be investigated using XFEM or by writing a subroutine based on the critical values of the energy release rates

REFERENCES

[1] Kinloch, A. J. "The science of adhesion." *Journal of Materials Science* 17.3 (1982): 617-651.

[2] Adams, R. D., and N. A. Peppiatt. "Stress analysis of adhesive-bonded lap joints." *The Journal of Strain Analysis for Engineering Design* 9.3 (1974): 185-196.

[3] Goland, Ma, and E. Reissner. "The stresses in cemented joints." *Journal of Applied Mechanics* 11.1 (1944): A17-A27.

[4] Zhu, Yuqiao, and Keith Kedward. *Methods of analysis and failure predictions for adhesively bonded joints of uniform and variable bondline thickness*. Office of Aviation Research, Federal Aviation Administration, 2005.

[5] Hart-Smith, Leonard John. *Adhesive-bonded single-lap joints*. Hampton, VA: Langley Research Center, 1973.

[6] Ojalvo, I. U., and H. L. Eidinoff. "Bond thickness effects upon stresses in single-lap adhesive joints." *AIAA Journal* 16.3 (1978): 204-211.

[7] Rodriguez, Rene Q., William P. Paiva, Paulo L. Sollero, Eder Albuquerque, and Marcelo B. Rodrigues. "Analytical and Numerical Tools for Bonded Joint Analysis." *Mecánica Computacional* XXIX (2010): 7557-569.

[8] D5573 Standard Practice for Classifying Failure Modes in Fiber-Reinforced-Plastic (FRP) Joints., 2012.

[9] Banea, M. D., and Lucas FM da Silva. "Adhesively bonded joints in composite materials: an overview." *Proceedings of the Institution of Mechanical Engineers, Part L: Journal of Materials Design and Applications* 223.1 (2009): 1-18.

[10] Talreja, Ramesh. "Defect damage mechanics: broader strategy for performance evaluation of composites." *Plastics, Rubber and Composites* 38.2-4 (2009): 49-54.

[11] Adams, R. D., and P. D. R. D. Cawley. "A review of defect types and nondestructive testing techniques for composites and bonded joints." *NDT International* 21.4 (1988): 208-222.

[12] Da Silva, Lucas FM, R. D. Adams, and M. Gibbs. "Manufacture of adhesive joints and bulk specimens with high-temperature adhesives." *International Journal of Adhesion and Adhesives* 24.1 (2004): 69-83.

[13] Liu, Ling, Ling, Bo-Ming Zhang, Dian-Fu Wang, and Zhan-Jun Wu. "Effects of cure cycles on void content and mechanical properties of composite laminates." *Composite Structures* 73.3 (2006): 303-309.

[14] Shahin, Khaled, and Farid Taheri. "The strain energy release rates in adhesively bonded balanced and unbalanced specimens and lap joints."*International Journal of Solids and Structures* 45.25 (2008): 6284-6300

[15] Rossettos, J. N., P. Lin, and Hamid Nayeb-Hashemi. "Comparison of the effects of debonds and voids in adhesive joints." *Journal of Engineering Materials and Technology* 116.4 (1994): 533-538.

[16] Chadegani, Alireza, and Romesh C. Batra. "Analysis of adhesive-bonded single-lap joint with an interfacial crack and a void." *International Journal of Adhesion and Adhesives* 31.6 (2011): 455-465.

[17] Suo, Zhigang, and John W. Hutchinson. "Interface crack between two elastic layers." *International Journal of Fracture* 43.1 (1990): 1-18.

[18] Ricotta, Mauro, Marino Quaresimin, and Ramesh Talreja. "Mode I strain energy release rate in composite laminates in the presence of voids." *Composites Science and Technology* 68.13 (2008): 2616-2623.

[19] Hoang-Ngoc, Cat-Tan, and Eric Paroissien. "Simulation of single-lap bonded and hybrid (bolted/bonded) joints with flexible adhesive." *International Journal of Adhesion and Adhesives* 30.3 (2010): 117-129.

[20] Callister, William D. *Fundamentals of Materials Science and Engineering: An Integrated Approach*. 2nd ed. Hoboken, NJ: John Wiley & Sons, 2005. 184. Print.

[21] Asp, L. E., Lars A. Berglund, and Ramesh Talreja. "A criterion for crack initiation in glassy polymers subjected to a composite-like stress state."*Composites Science and Technology* 56.11 (1996): 1291-1301.

[22] Rybicki, E. Fo, and M. F. Kanninen. "A finite element calculation of stress intensity factors by a modified crack closure integral." *Engineering Fracture Mechanics* 9.4 (1977): 931-938.

[23] Krueger, Ronald. "Virtual crack closure technique: history, approach, and applications." *Applied Mechanics Reviews* 57.2 (2004): 109-143.

[24] Williams, M. L. "The stresses around a fault or crack in dissimilar media."*Bulletin of the Seismological Society of America* 49.2 (1959): 199-204.

[25] Valvo, Paolo S. "A revised virtual crack closure technique for physically consistent fracture mode partitioning." *International Journal of Fracture* 173.1 (2012): 1-20.

[26] Kafkalidis, M. S., and M. D. Thouless. "The effects of geometry and material properties on the fracture of single lap-shear joints." *International Journal of Solids and Structures* 39.17 (2002): 4367-4383.

[27] Camanho, Pedro P. *Mechanical Response of Composites*. Dordrecht: Springer, 2008. 107. Print.

[28] Hadj-Ahmed, Réda, Gilles Foret, and Alain Ehrlacher. "Probabilistic analysis of failure in adhesive bonded joints." *Mechanics of Materials* 33.2 (2001): 77-84.